Nanoscale Advances

ROYAL SOCIETY OF CHEMISTRY

REVIEW

View Article Online
View Journal | View Issue

Cite this: *Nanoscale Adv.*, 2024, **6**, 2741

Nanocosmos of catalysis: a voyage through synthesis, properties, and enhanced photocatalytic degradation in nickel sulfide nanocomposites

Nityananda Sarkar, Soumya Ranjan Mishra, Vishal Gadore, Biswaranjan Panigrahi and Md. Ahmaruzzaman *

Nanomaterials play a decisive role in environmental applications such as water purification, pollutant monitoring, and advanced oxidation-based remediation processes, particularly in semiconductor and metal sulfide-based photocatalysis. Metal sulfides are ideal for photocatalysis because of their unique optical, structural, and electronic characteristics. These properties enable the effective use of solar energy to drive various catalytic reactions with potential uses in environmental remediation with sustainable energy production. Among them, nickel sulfides (NiS) stand out for their narrow band gaps, high stability, and cost-effectiveness. This review thoroughly analyzes recent advancements in employing nickel–sulfide-based nanostructures for water decontamination. It begins by addressing environmental material needs and emphasizing the properties of nickel sulfide. To improve photocatalytic performance, controlled processes that affect the active structure, shape, composition, and size of nickel sulfide photocatalysts are examined, along with their synthesis methods. The heart of the review article is a detailed analysis of the modification of NiS through metal and non-metal doping, heterojunction, and nanocomposite formation for enhanced photocatalytic performance. The discussion also includes metal-modified nanostructures, metal oxides, and carbon-hybridized nanocomposites. This study underscores notable advancements in the degradation efficiency of NiS photocatalysts, rivaling their costly noble-metal counterparts. The analysis concludes with potential future directions for nickel sulfide-based photocatalysts in sustainable environmental remediation.

Received 3rd March 2024
Accepted 6th April 2024

DOI: 10.1039/d4na00184b

rsc.li/nanoscale-advances

1. Introduction

Water is a vital resource necessary for maintaining life, and its pollution poses a significant threat to both ecosystems and human well-being. From the moment we wake up to when we go to bed, water plays an integral part in our daily routines, impacting our health, hygiene, nutrition, and leisure activities.[1] Water pollution occurs when harmful substances are introduced into various water sources, such as rivers, lakes, oceans, and groundwater. These substances include dyes, pharmaceutical products, and pesticides, which can adversely affect aquatic life and the environment.[2] Industrial discharge of dyes introduces harmful chemicals into water sources, which can negatively impact aquatic life.[3] Moreover, pharmaceuticals can contaminate water supplies if not disposed of properly, posing risks to aquatic organisms and human health.[4] Also, pesticides used in agriculture to control pests often end up in water bodies through runoff, causing ecological imbalances and potentially harming aquatic ecosystems. To mitigate the negative effects of these substances on water quality and the environment, there is a need for stringent regulations, proper waste management, and sustainable practices.[5] Scientists have proposed various physical, chemical, and biological treatment approaches to address these issues.[6] Chemicals like dyes, pesticides, and medications can be removed from wastewater using nanocomposites, composite materials made of two or more components, one acts as the basis material and includes the other ingredients.[7] Nickel sulfide nanocomposites have gained recognition for their remarkable effectiveness in eliminating dyes, pharmaceuticals, and pesticides from wastewater, with several instances reviewed in this study. These studies also highlight recent advancements in nickel sulfide (NiS) nanocomposite materials to eliminate organic contaminants.[8]

Using light energy to catalyze chemical processes is known as photocatalysis, which comes from the Greek words “phos” (light) and “katalyo” (catalysis or breakdown). Energy conversion, environmental cleanup, and the development of sustainable technologies all depend on this scientific method.[9] Photocatalysts play a crucial role in the breakdown of chemicals, including pesticides, dyes, and medicines, as well as in the purification of air and water. The creation of solar fuel is a noteworthy use of photocatalysis. When a photocatalyst is exposed to UV or visible light, electron–hole pairs are created,

Department of Chemistry, National Institute of Technology Silchar, Assam, 788010, India. E-mail: mda2002@gmail.com

which changes the rate at which a chemical reaction proceeds.[10,11] The photocatalysis process unfolds through several fundamental steps. Initially, a semiconductor material first excites electrons from the valence band to the conduction band by absorbing photons. Electron–hole pairs, which function as the active species in chemical reactions, are produced by this process. Subsequently, the electrons possess the capability to reduce specific species, whereas the holes exhibit the ability to oxidize others. This distinctive dual functionality involving oxidation and reduction stands out as a defining characteristic of photocatalysis. Fig. 1 (ref. 12) illustrates the mechanism of photocatalytic degradation of dyes.

In aqueous environments, the h^+ reacts with water molecules, creating *OH, while e^- reacts with O_2 molecules, forming O_2^{*-} radicals. These reactive oxygen species play a decisive role in breaking down pollutants. The intermediate species formed during photocatalysis react with organic contaminants, breaking them into more straightforward, less harmful compounds. This process results in the degradation and removal of pollutants from the environment.[13] The chemical reactions are depicted in Fig. 2.[7]

1. The photoexcitation of semiconductor takes place,
$$SC + hv \rightarrow e^- + h^+$$
2. Ionosorption of oxygen takes place,
$$O_2 + e^- \rightarrow O_2^{*-}$$
3. Followed by ionization of water,
$$H_2O \rightarrow OH^- + H^+$$
4. The hydroxyl ion gets oxidised,
$$OH^- + h^+ \rightarrow {}^*OH$$
5. The superoxide gets protonated,
$$O_2^{*-} + H^+ \rightarrow HO_2^*$$
6. Followed by co-scavenging of electron,
$$HO_2^* + e^- \rightarrow HO_2^-$$
7. Formation of hydrogen peroxide,
$$HO_2^- + H^+ \rightarrow H_2O_2$$
8. Followed by *OH formation,
$$H_2O_2 + e^- \rightarrow {}^*OH + OH^-$$
9. The pollutants get degraded by active species,
$$\text{Pollutant} + {}^*OH \rightarrow \text{degradation product}$$
$$\text{Pollutant} + h^+ \rightarrow \text{oxidation product}$$
$$\text{Pollutant} + e^- \rightarrow \text{reduction product}$$

Fig. 2 Chemical reactions involved in the photocatalytic degradation.[7]

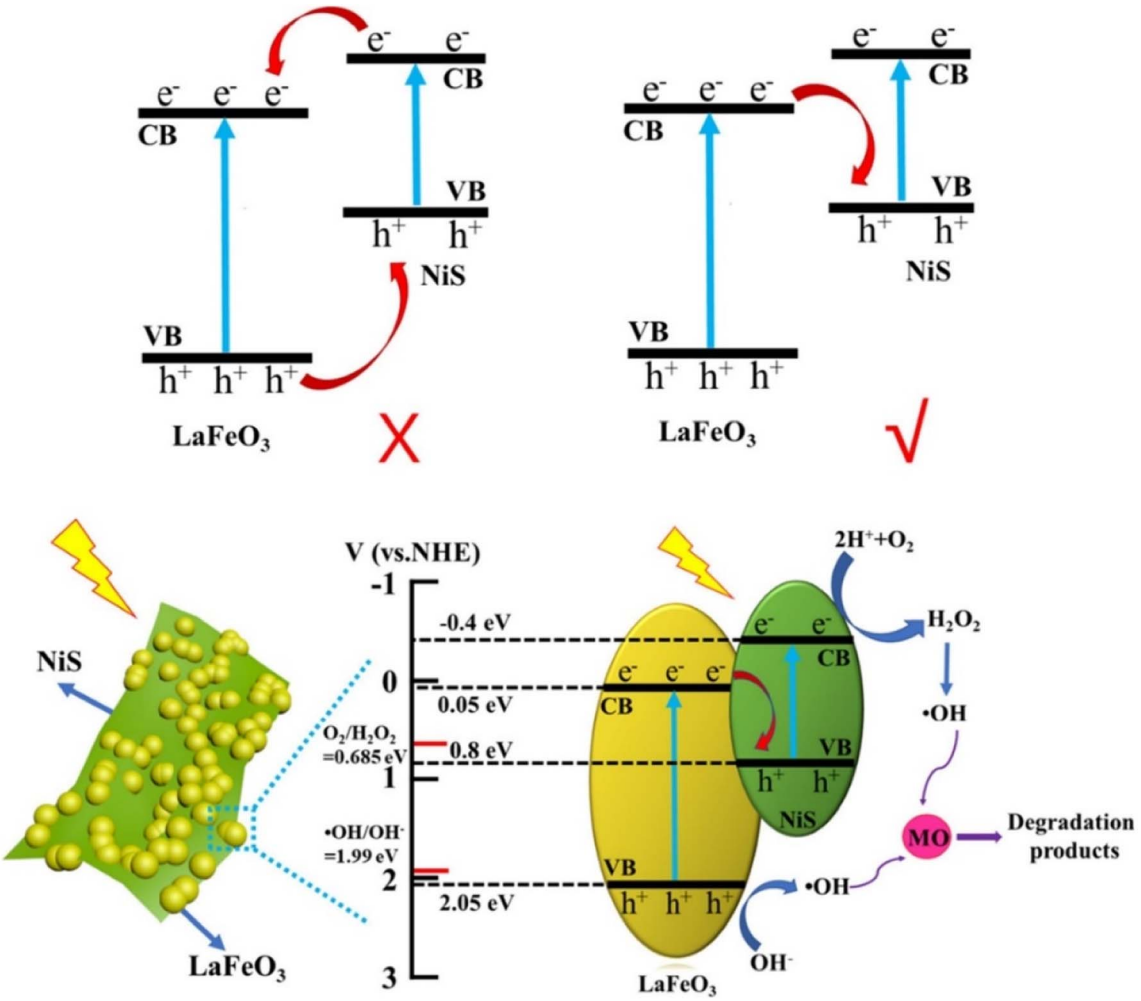

Fig. 1 Schematic diagram showing how NiS/LFO heterostructures photocatalytically degrade MO.[12]

Overall, photocatalysis relies on the ability of a semiconductor material, activated by light, to initiate and drive redox reactions that lead to the decomposition of pollutants and the purification of air or water. The most commonly used semiconductor materials for photocatalysis are titanium dioxide, zinc oxide, and various metal sulfides.[14] Nickel sulfide (NiS) is a remarkable material in photocatalysis, outperforming other metal sulfides and well-known photocatalysts. NiS outperforms its competitors in various ways due to its unique electrical structure and high catalytic activity.[15] Unlike certain metal sulfides, which may have restricted light absorption or poor charge separation efficiency, NiS has an optimized band structure that effectively exploits a larger spectrum of light for improved photocatalytic activity.[16] This intrinsic advantage places NiS at the forefront of solar-driven catalysis.[17]

Compared to other well-known photocatalysts, its extraordinary properties become even more apparent. Compared to traditional photocatalysts like titanium dioxide (TiO_2), zinc oxide (ZnO), molybdenum disulfide (MoS_2), cadmium sulfide (CdS), or tin disulfide (SnS_2),[1,10,14,18–24] NiS exhibits better catalytic activity in visible light, accounting for a significant fraction of the solar spectrum. Its ability to capture visible light broadens its application potential and overcomes a key restriction shared by many photocatalysts that absorb mostly UV light. NiS's high photocatalytic efficiency makes it an attractive contender for tackling environmental issues and promoting sustainable energy solutions.[17] In addition to their inherent strength, NiS-based composites have a significant advantage in photocatalytic degradation. When combined with other materials, such as graphene, carbon nanotubes, or other metal oxides, synergistic effects improve total photocatalytic activity.[25] These composites use each component's strengths, such as better charge separation, prolonged light absorption, and more excellent stability, to create a material that outperforms the individual capabilities of its parts.[20] As a result, utilizing NiS-based composites provides a sophisticated way to obtain greater photocatalytic efficiency, making them highly appealing for applications ranging from wastewater treatment to solar fuel production.

Finally, the superiority of NiS as a photocatalyst, both as a standalone material and as part of composite materials, places it at the forefront of the field. It is distinguished from other metal sulfides and well-known photocatalysts by its optimized electronic structure, effective light absorption, and remarkable catalytic activity.[26] NiS stands out as a vital participant in expanding photocatalysis science as the scientific community continues investigating novel solutions for environmental concerns and sustainable energy generation. In this review article, nickel sulfide's synthesis techniques, properties, and characteristics are discussed. Furthermore, the review paper analyzes the enhancement in photocatalytic properties due to several modifications to it and discusses the recent advances in the field of photocatalytic degradation. The review paper ends by giving a future perspective for upcoming research works and sheds light on the forthcoming challenges for better performance.

2. Synthesis of nickel sulfides and their nanocomposites

Several traditional techniques have been documented for producing nanoparticles and nanocomposites made of nickel sulfide. Here are several often-used, straightforward synthesis techniques in this context. Fig. 3 (ref. 10) presents a schematic representation of the synthesis procedures.

2.1 Sol–gel method

Metal sulfides may be made quickly and efficiently using the sol–gel process. A metal salt precursor is first dissolved in a solvent, and then a sulfur source, typically sodium sulfide, is added to the mixture to produce a sol. The metal sulfide sol condenses into a gel of metal–sulfur–metal bonds after it forms. After that, the gel is dried for future use.

As an example, sol–gel synthesis of the NiS_2 nanocomposite involved the combination of $NiCl_2$ with $Na_2S\cdot 5H_2O$ in water for the subsequent creation of the NiS_2/TiO_2 composite. The resulting NiS_2 powder was incorporated into a 1 : 4 TNB and benzene solution. This mixture underwent homogenization at 80 °C for 10 h using a shaking water bath with a shaking rate set at 120 rpm. After homogenization, the composite was subjected to drying at 100 °C. A thermal heat treatment was applied at 500 °C for 1 h. The catalyst was further processed by grinding in a ball mill and designated sg-NiS_2/TiO_2. Furthermore, it is noteworthy that the sol–gel technique is versatile and allows for adding metal and non-metal dopants to the system.[27]

2.2 Hydrothermal method

One popular synthesis method for creating nanoparticles with various surface morphologies and porosities is the hydrothermal approach. In this procedure, a Teflon-lined hydrothermal autoclave containing an aqueous solution of metal salt and a sulfur source is heated to high temperatures. The final product's morphology may be accurately controlled by varying variables, including temperature, pH, time, and pressure.

In order to create a homogenous solution for the hydrothermal production of NiS nanoparticles, a combination of $NiSO_4$ (10 mmol), NaOH (15 mmol), TAA (12 mmol), and 180 mL of distilled, deionized water was stirred. The final combination was then heated for 24 h at 160 °C in a hot air oven and sealed in a 200 mL autoclave lined with Teflon. The reaction mixture then cooled down to room temperature on its own. Centrifugation separated the resultant solution, and ethanol and deionized water were used repeatedly to wash it. In the last stage, the solution was dried at 70 °C in a dust-free atmosphere, which produced a black powder.[28]

2.3 Solvothermal method

Similar in nature to the hydrothermal method, the solvothermal approach substitutes an organic solvent—typically *N*,*N*-dimethylformamide—for water. To create a homogenous suspension, a certain amount of metal salt must dissolve in the solvent. After that, the mixture is heated in an autoclave with a Teflon

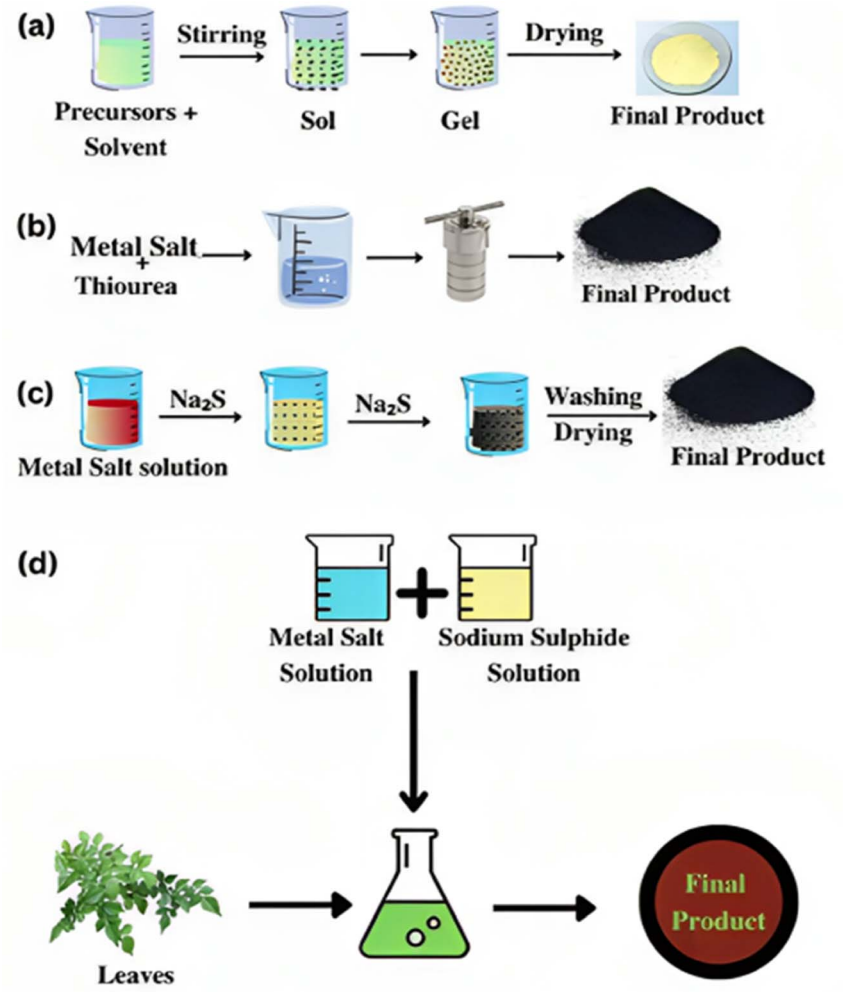

Fig. 3 Graphical depiction of the (a) sol–gel, (b) hydrothermal, (c) precipitation, and (d) green synthesis methods.[10]

lining and a sulfur source. The precipitate is next put through centrifugation, careful washing, and drying procedures to get the finished product.

To make NiS/rGO nanocomposite, sonication combined 1 gm of graphene oxide (GO) with 40 mL of ethylene glycol to generate a homogenous slurry. The GO dispersion was constantly stirred while 0.2 gm of lab-synthesized NiS nanoparticles were added. These had been made using the solvothermal process and dissolved in 20 mL of ethylene glycol. Subsequently, 0.1 M NaOH solution to 5 mL of distilled water was added and vigorously mixed the blend for 30 min. The solution was placed in an autoclave and heated to 160 °C for 48 h after full dispersion. The final mixture was dried for 24 h at 60 °C after being repeatedly cleaned with ethanol and deionized water. A black powder was obtained.[29]

2.4 Precipitation and co-precipitation method

The precipitation method is considered the most straightforward synthesis technique, eliminating the need for high temperatures and following standard procedures. This method is beneficial for producing metal sulfide nanocomposites, as it allows the simultaneous precipitation of two or more metal sulfides. Inorganic metal salts undergo precipitation during this procedure by introducing sodium sulfide with vigorous stirring. The resultant particles exhibit a broad size distribution, ranging from nanometers to micrometers. Achieving a consistent particle size may necessitate milling the final product.

The synthesis of NiS/Ag_2MoO_4 required ultrasonication in a water/ethanol combination at a 1 : 1 ratio. While the sonication was going on, 0.1 M $AgNO_3$ was added. Following that, 0.05 mol of sodium molybdate ($Na_2MoO_4 \cdot 2H_2O$) solution was created. The $Na_2MoO_4 \cdot 2H2O$ solution was rapidly added after the 2 h sonication, and the mixture was vigorously stirred for an additional half-hour. To get the final result, the collected sample was repeatedly cleaned with ethanol and water before being dried at 80 °C.[30]

2.5 Green synthesis method

Researchers have recently emphasized the environmentally friendly synthesis of nickel sulfides, prioritizing using plant or microbial extracts as a source of sulfur. These extracts serve as

both capping and stabilizing agents, aligning with the principles of green chemistry. The green synthesis approach for nickel sulfides has demonstrated improved photocatalytic and antibacterial properties. The biological process, known as "green synthesis," is gaining popularity as an eco-friendly, cost-effective, and non-toxic alternative for producing NiS nanoparticles (NPs). This method leverages natural ingredients like plant extracts and microbes, contributing to improved stability in the synthesis process.

To illustrate this method, a solution containing L-cysteine (L-cys, 7.5 mmol) and $NiCl_2 \cdot 6H_2O$ (1.5 mmol) in 50 mL of deionized water was introduced to a 30 mL suspension of graphene oxide sheets (3 mmol) under vigorous stirring for 2 h. The mixture was then put into a 100 mL stainless steel autoclave that was firmly sealed, lined with Teflon, and heated to 200 °C for 24 h. After that, the autoclave was left to cool naturally to ambient temperature. After centrifugation, the resultant black precipitate was collected and repeatedly cleaned with ethanol and deionized water. Lastly, the NiS_2/graphene composites were dried for a period of 12 h at 80 °C in a vacuum oven.[31]

In conclusion, sol–gel, hydrothermal, precipitation, and green synthesis methods are diverse approaches to fabricating nanomaterials, each offering distinct advantages. Sol–gel methods provide precise control over composition and morphology, while hydrothermal processes facilitate the growth of well-defined nanostructures. Precipitation methods are valued for their simplicity and scalability. Using environmentally friendly routes, green synthesis techniques stand out for their sustainable and eco-friendly characteristics. The choice of method depends on specific application requirements, emphasizing the importance of tailoring synthesis approaches to achieve desired nanomaterial properties. The benefits and drawbacks of the various synthesis techniques discussed above are shown in Table 1 below.

3. Structural properties

Nanostructured materials, encompassing nanowires, nanotubes, nanobelts, and nanorods, have captured considerable scientific interest due to their distinctive physicochemical properties and versatile applications across diverse domains. The investigation of these nanostructures' magnetic, electronic, and optical features has emerged as a central focus, driven by the unique attributes that set them apart from their bulk counterparts.[32]

In this context, metal sulfides, including nickel sulfide, are notable for their captivating electronic properties, opening avenues for various technological applications. Nickel sulfide has garnered significant interest due to its potential role as a transformation toughening agent in semiconductors, catalysts, and cathodes for rechargeable lithium batteries.[10]

Binary Ni–S systems, including $Ni_{3+x}S_2$, Ni_3S_2, Ni_4S_{3+x}, Ni_6S_5, Ni_7S_6, Ni_9S_8, NiS, Ni_3S_4, and NiS_2, have also piqued interest due to their multi-phase nature. Depending on temperature, nickel sulfide can adopt two crystal structures, α, and β.[33]

Fig. 4a (ref. 34) shows that α-NiS has an arsenide-like hexagonal structure. In this configuration, six sulfur atoms encircle each nickel atom octahedrally. A considerable degree of metal–metal bonding is indicated by the proximity of two additional nickel atoms to each nickel atom, resulting in a Ni–Ni distance of around 2.68 Å. Cubic NiS_2, which has a pyrite structure, is another common form of nickel sulfide (Fig. 4b).[34] Discrete S units are present in this structure, and the S–S distance inside these units is very similar to the S–S distance of a single S–S bond. The overall structure may be considered a deformed NaCl structure, with nickel atoms occupying Na-like places and S_2 groups arranged so that the Cl positions correspond to the cores of the groups. The structure of Ni_3S_2 is rhombohedral, as seen in Fig. 4c.[34] Each nickel atom in this

Table 1 Pros and Cons of the synthesis methods for fabrication of nickel sulfide

Synthesis methods	Advantages	Disadvantages
Sol–gel	• Homogeneous and pure products	• Lengthy processing time and intricate methodology
	• Control over composition and low-temperature processing	• Shrinkage and cracking
Hydrothermal	• Easy and cost-effective	• High energy consumption due to long reaction time
	• Fabrication of high-quality nanomaterials with excellent morphology, particularly nanorods	• Instrumental and material incompatibility
Solvothermal	• Synthesis of narrow-size distributed nanomaterials	• Complex equipment requirements
	• Versatility to a wide range of materials, including metals, metal oxides, and organic-inorganic hybrids	• Limited to certain solvents
Precipitation and co-precipitation method	• Simple, cost-effective, and used for large-scale production	• Difficulty in controlling stoichiometry leads to the formation of unwanted phases
	• Less reaction times	• Difficulty in controlling particle size
Green synthesis	• Environmentally friendly due to the use of non-toxic reagents	• Slower reaction rates
	• Low energy consumption	• Limited control over particle size

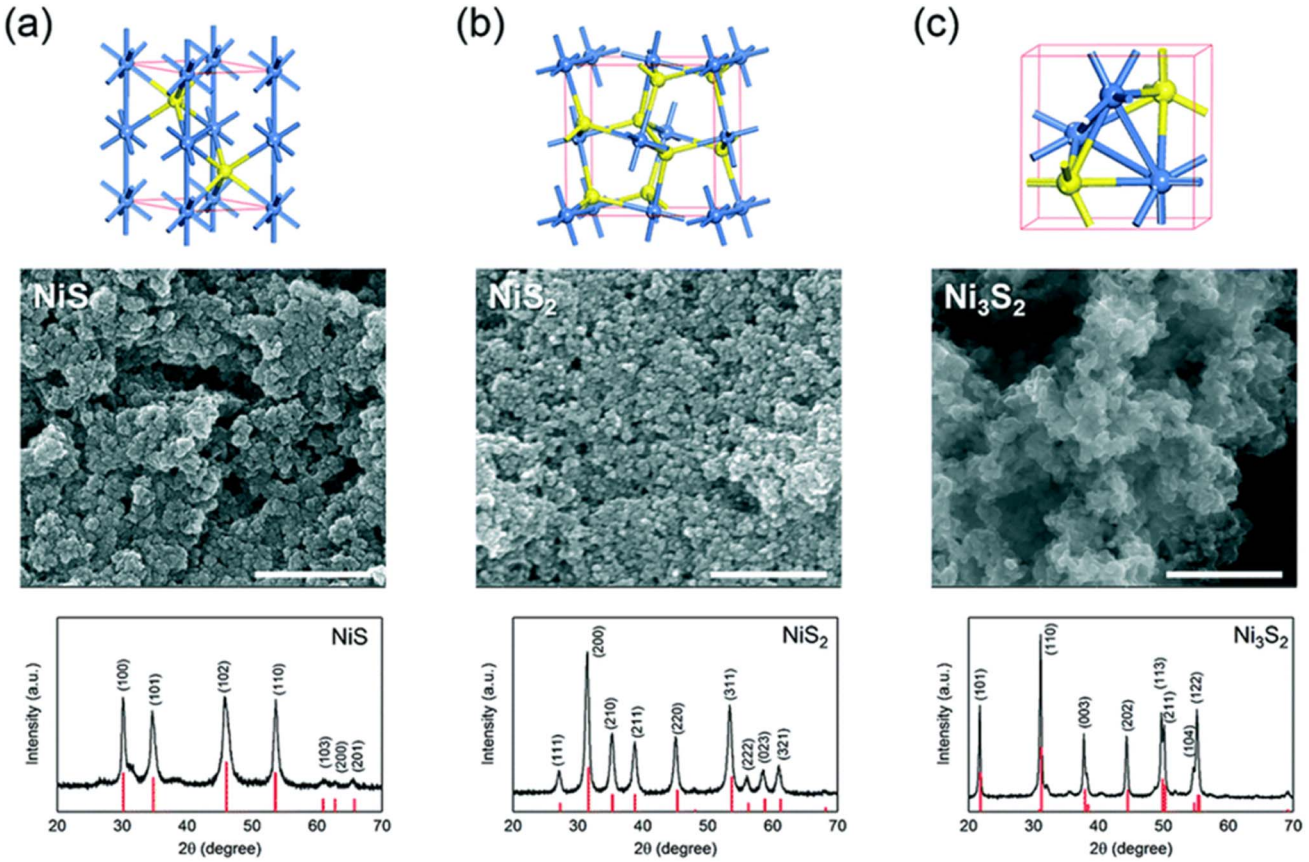

Fig. 4 The unit cell structures, scanning electron microscopy (SEM) images, and X-ray diffraction (XRD) patterns of three nickel sulfides— (a) α-NiS, (b) NiS_2, and, (c) Ni_3S_2. The red vertical lines in each XRD panel indicate the theoretical pattern.[34]

configuration is located in a pseudo-tetrahedral site inside a cubic sulfur lattice that is about body-centered. There are noteworthy metal–metal bonding interactions between nickel atoms due to the short Ni–S (2.29 Å) and Ni–Ni (2.53 Å) lengths that connect the Ni_3S_2 units. Fig. 4c also shows the highlighted trigonal bi-pyramidal core of Ni_3S_2.[34]

Additionally, the rhombohedral unit cell structure, morphology, and XRD patterns of β-NiS are depicted in Fig. 5a–d, with all peaks corresponding to β-NiS. The X-ray diffraction (XRD) (Fig. 5a) analysis did not detect any discernible diffraction peaks arising from additional impurities such as Ni_2S_3, Ni_3S_4, or Ni_9S_8. The observed space group for the prepared materials is $R3m$, with cell parameters approximately $a = 9.62$ Å and $c = 3.15$ Å, consistent with literature values (card no. 12-0041). Moreover, Fig. 5c and d showcases the overall morphology of the product, indicating that the morphology retains nanorod-based flower-like architectures. A closer examination of the high-magnification SEM image reveals that the nanorods grow more compactly, resembling a sphere, with some flutes appearing at the side planes of the nanorods.[35]

A diverse array of nickel sulfide nanoparticles, including nanospheres, nanorods, nano prisms, nanoneedles, hollow spheres, flower-like architectures, urchin-like nanocrystalline, and layer-rolled structures, has been successfully produced using various methods such as hydrothermal, solvothermal, molecular procedures, and precipitation routes. Nevertheless, the impact of nanoparticle morphologies on their physicochemical behavior underscores the pressing necessity for additional endeavors in attaining a tunable synthesis of uniformly shaped nickel sulfide nanoparticles.[19]

Nickel sulfide (NiS) stands out among metal sulfide-based photocatalysts because it possesses the smallest bandgap (1.92–2.41 eV, Fig. 6),[36] making it a favorable choice for preparation, as lower band gaps enhance light absorption, charge separation efficiency, and redox activity, thereby improving photocatalytic properties. The structural characteristics of NiS contribute to its distinctive properties in the field of photocatalysis.[10] NiS typically adopts a crystalline structure, and its narrow bandgap allows NiS to efficiently absorb light in the visible spectrum, promoting enhanced photoexcitation and facilitating photocatalytic reactions under sunlight.[37]

To validate the elemental composition, XPS analysis was carried out. The typical survey spectra of NiS are shown in Fig. 5a, where the binding energies are calibrated using the reference value of the C (1s) peak at 284.6 eV. Ni $2p_{3/2}$ and Ni $2p_{1/2}$ are responsible for the notable peaks at 853.0 and 873.2 eV, respectively. Peaks at 162.4 and 167.7 eV are associated with S $2p_{3/2}$ and S $2p_{1/2}$ binding energies. The system exhibits electron correlation as seen by the two strong satellite peaks for Ni $2p_{3/2}$ and Ni $2p_{1/2}$, located at around 860.6 and

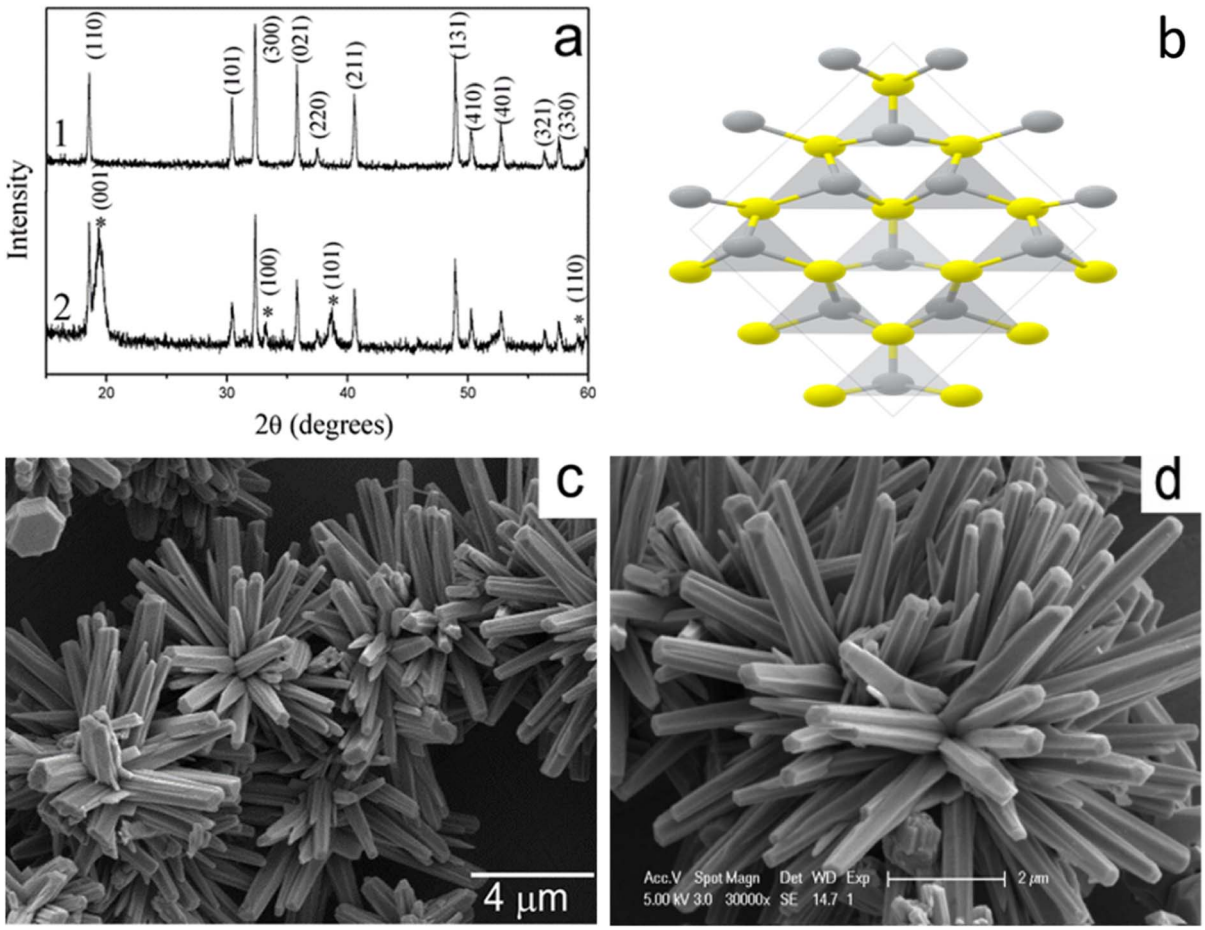

Fig. 5 (a) X-ray diffraction (XRD) patterns, (b) unit cell structures, and (c and d) scanning electron microscopy (SEM) images of β-NiS.[35]

878.9 eV, respectively. This discovery further confirmed the elemental makeup and electrical structure of the NiS sample. All sample's UV-visible absorption characteristics were measured.

The figure (inset in Fig. 6b) revealed that the band gaps for Ni6, Ni9, and Ni12 were 2.05, 1.92, and 2.4 eV, respectively. Notably, the band gap was observed to be dependent on the concentration of sodium dodecyl sulfate (SDS). Diffuse reflectance spectra (DRS) were measured to examine the photoabsorption properties, with barium sulfate as the reference. All samples exhibit high absorption in the UV-visible region (200–800 nm).[36]

Following the second and fourth runs, the recycled Ni12's DRS spectrum showed almost little change in absorption characteristics. With more catalytic cycles, there was a trend toward decreased reflectance intensity, which might be related to sample thickness (during DRS sample preparation), catalyst loss (8–10%), and the adsorption of photodegraded dye on nanoparticles.[36]

The morphological characteristics of nickel sulfide nanoparticles are illustrated in Fig. 7.[36] Distinct morphologies emerge based on varied reaction conditions during sample preparation. Ni1, Ni3, Ni4, and Ni5 exhibit a spherical structure, while Ni2 displays a mixed morphology with network and sphere-like structures. Ni6 has bigger-sized particles, but the morphologies of Ni7 and Ni8 are more like networks. Ni9 and Ni10 samples heated to 80 °C show irregular shapes and sizes and aggregated particle morphologies. Notably, Ni12 exhibits a sponge-like morphology. Hydrophilic interactions, van der Waals forces, electrostatic and dipolar fields inside the aggregate, crystal-face attraction, and hydrogen bonds significantly impact the changes in sample morphology when varying the capping agents. These elements probably function in concert to control the process of self-assembly that results in the final structure. The self-assembly process leading to the final structure is likely governed by a combination of these factors. TEM analysis confirms that Ni12 has a sponge-like morphology composed of tiny nanoparticles, but Ni9 and Ni2 have heterogeneous shapes (Fig. 7b–e). EDX results for all samples confirm the presence of Ni and S. Spatial regularity in the elemental distribution of Ni12 reveals a composition of $Ni_{0.8}2S_{1.00}$. The Ni and S homogenous distribution throughout the Ni12 sample is further shown by EDX elemental mapping and line scanning (Fig. 7a).[36]

In conclusion, nickel sulfide nanoparticles' diverse crystal structures and morphologies, ranging from hexagonal to sponge-like, highlight their versatility and tunable synthesis capabilities. The unique electronic properties of nickel sulfide, especially its small bandgap, make it a promising material for

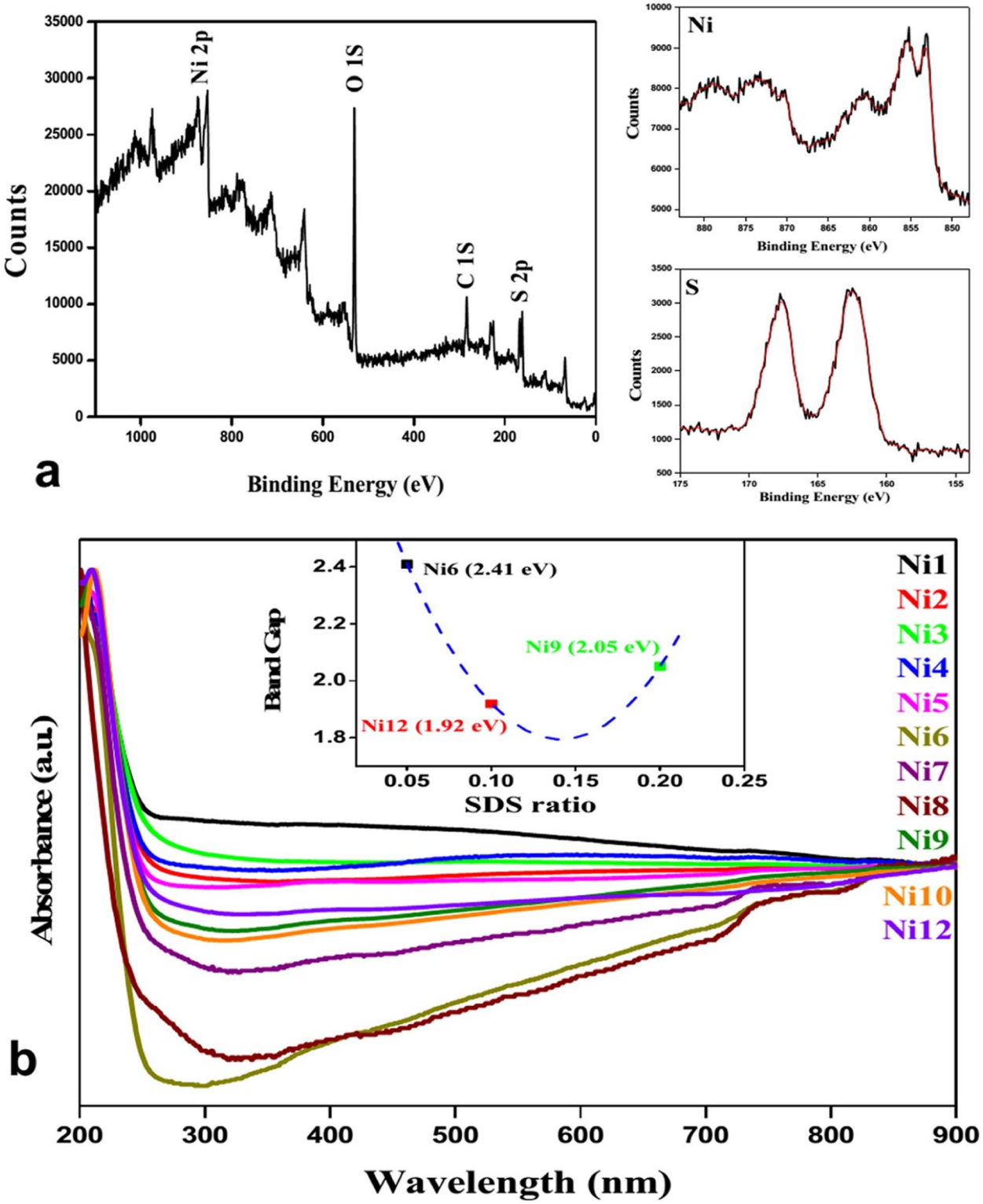

Fig. 6 (a) XPS spectra of NiS; (b) Uv-visible spectroscopy and band gap determination (inset) for nickel sulfide nanoparticles.[36]

various technological applications, including photocatalysis and rechargeable lithium batteries. The comprehensive characterization through XPS, UV-visible spectroscopy, and electron microscopy provides valuable insights into the elemental composition, electronic structure, and morphological features of different nickel sulfide nanoparticles. Further exploration of these nanostructures holds great potential for advancing their applications in emerging fields.

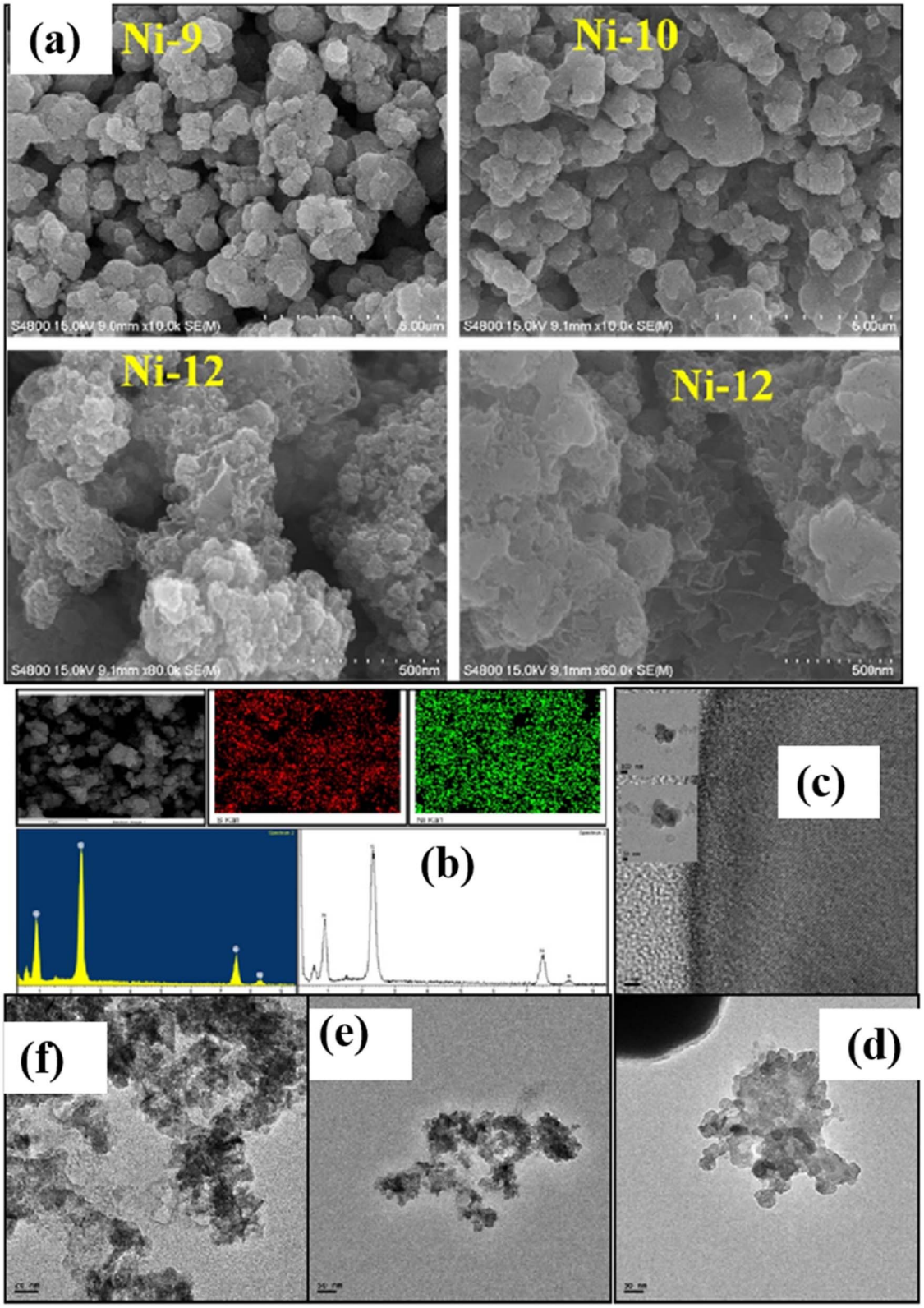

Fig. 7 (a) Field-emission scanning electron microscope (FE-SEM) images of nickel sulfide nanoparticles (NPs) with compositions Ni9, Ni10, and Ni12; (b) energy-dispersive X-ray (EDX), mapping, and line scanning specifically for Ni12; transmission electron microscope (TEM) images showcase (c) Ni2, (d) Ni9, and (e and f) Ni12.[36]

4. Enhancement of photocatalytic efficiency

4.1 Doping

Doping is a technique that involves the insertion of impurities into a semiconductor to improve conductivity. This process introduces defect states into the band gap, which helps prevent fast charge recombination while allowing visible light absorption. Two scenarios arise in this situation, where charge recombination is slowed in the first case, and interfacial charge transfer is increased by trapping valence band (VB) holes or conduction band (CB) electrons at defect sites. In the second case, sub-bandgap irradiation facilitates electronic transitions from defect states to CB or VB to defect states.[38]

There are various doping types, such as metal doping, nonmetal doping, co-doping, and metalloid-halogen doping. The principal dopants are metal ions, including transition metals, noble metals, and nonmetal ions. Selective metals are often picked for their ability to transport electrons and lower the band gap energy level.[39] When metal ions are activated in the presence of a light source, electron holes are generated in doped catalysts. Metal ion dopants in the photocatalyst matrix considerably improve interfacial electron transport and decrease charge carrier recombination rates, increasing photo reactivity.[40]

Doping was required to improve conductivity in the case of pure nickel sulfide, which had low efficiency because of limited light absorption and significant charge separation. Overall, photodegradation efficiency was enhanced with doping by slowing the recombination of photo-generated charges and broadening the visible light absorption spectrum.[41]

4.1.1 Metal doping. The enhancement of binding functions in a doped system by metallic impurities is critical for reducing bandgap and improving visible light absorption, boosting efficiency. As a result, charge carriers are more efficiently transferred, transported, and separated, which is essential for causing a spatial distribution of charge carriers that promotes photocatalytic processes.[40]

The production of electron–hole pairs is essential for reactions involving species adsorbed on the surface of the photocatalyst in terms of photocatalytic efficiency.[32] Doped catalysts produce electron holes by using activated metal ions and a light source. Thus, by reducing charge carrier recombination rates and increasing interfacial electron transfer rates, adding metal ion dopants to the photocatalyst matrix increases photoreactivity. It's important to remember that metal dopants also help doped NiS exhibit improved morphology.[38]

Different transition metals are utilized as dopants in nickel sulfide (NiS) photocatalysts to modify the semiconductor's characteristics. Transition metals such as iron (Fe), cobalt (Co), chromium (Cr), manganese (Mn), barium (Ba), platinum (Pt), zinc (Zn), cerium (Ce), vanadium(v), gold (Au), and silver (Ag) are frequently utilized for metal doping in NiS photocatalysts. These metal dopants improve photocatalytic activity by raising light absorption, lowering the bandgap, speeding up charge mobility, and lengthening the lifespan of charge carriers.[40] Doping with metal introduces impurity band energy levels, causing a reduction in the gap between the valence band and conduction band, as illustrated in Fig. 8.

For instance, Manikandan *et al.*[42] synthesized Mn^{2+} doped NiS and found that the concentration of metal doping influences the average size and form of $Mn_xNi^{1-x}S$ nanocrystals. The E_g of the undoped NiS is 2.05 eV, and when Mn^{2+} ions ($x = 0.3$–0.5) are added, it rises from 2.19 to 2.31 eV. Additionally, the produced materials showed remarkable catalytic and optomagnetic characteristics. The $Mn_xNi^{1-x}S$ nanocrystals produced have demonstrated modest ferromagnetic activity in their M − H loop. Because Mn^{2+} ions have a greater magnetic moment ($5\mu_B$) than Ni^{2+} ions ($2\mu_B$), the M_s values rise as the concentration of Mn^{2+} ions increases. Furthermore, it has been shown that the samples' surface area rises with increasing Mn concentration ($x = 0.0$–0.5), with $Mn_{0.5}Ni_{0.5}S$ having a greater surface area (69.47 $m^2\ g^{-1}$) than undoped NiS. Consequently, $Mn_{0.5}Ni_{0.5}S$'s large surface area improves its photocatalytic capabilities. Photocatalysts provide more excellent surface-active sites with a high specific surface area, which enhances photocatalytic activity. The dispersion of particles per volume in the solution rises as the particle size decreases. Photon absorbance is improved due to increased active surface sites and photoactive centers.[42]

Incorporating transition metal dopants, such as Mn^{2+}, in NiS photocatalysts is crucial in modifying their band structure, reducing the band gap, and enhancing visible light absorption. This improves photocatalytic efficiency through increased

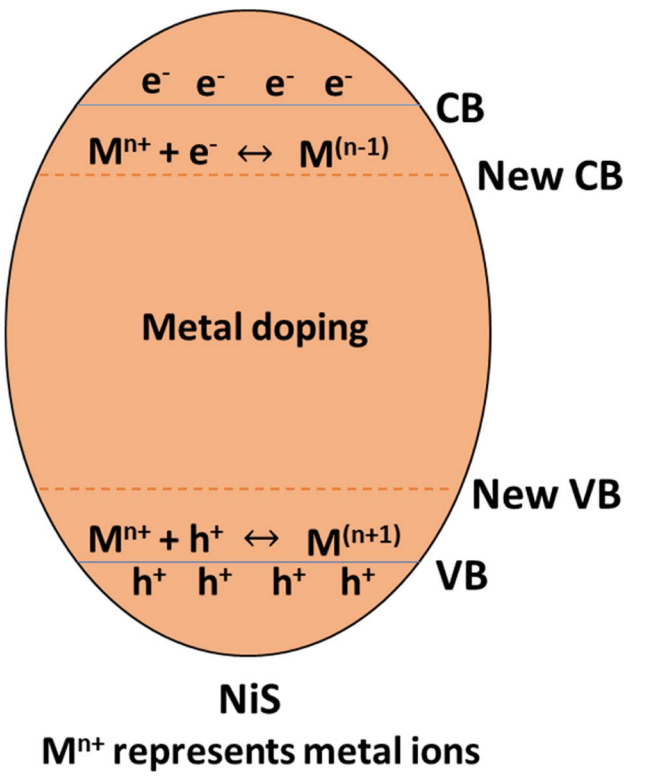

Fig. 8 Schematic illustration of band structure modification due to metal doping.

charge carrier mobility, reduced recombination rates, and extended carrier lifespans. The concentration of metal dopants also influences nanocrystal size, catalytic characteristics, and magnetic properties, with $Mn_{0.5}Ni_{0.5}S$ exhibiting notable enhancements in surface area, photocatalytic capabilities, and ferromagnetic activity, demonstrating the multifaceted impact of metal doping on NiS-based materials.

4.1.2 Nonmetal doping. Because of the advantages of non-metal doping, such as its high ionization energies and electronegativity, researchers are growing more and more interested in this technique. Covalent bonds are formed when non-metals interact with other molecules and pick up an electron. These covalent bonds provide thermal stability. Non-metal doping is preferred over metal doping because metal doping exhibits thermal fluctuations of chemical states, while non-metal doping does not.[32]

Doping nickel sulfide (NiS) with non-metal elements like phosphorus (P), oxygen (O), nitrogen (N), boron (B), and carbon (C) introduces a range of modifications to the semiconductor's properties, which significantly affect its photocatalytic behavior. For instance, phosphorus doping can alter the electronic structure and bandgap, affecting light absorption in the visible range. Oxygen doping can generate O_2 vacancies concerning the material's surface reactivity and charge carrier dynamics.[43]

Nitrogen doping is the most significant of all non-metal dopants because it increases light absorption into the visible range by widening the bandgap's energy range. This increases the activity of photocatalysis, especially when exposed to light. Boron doping modifies the electrical structure of nickel–silver and enhances charge separation efficiency, whereas carbon doping can modify surface properties and boost charge carrier mobility.[44]

Strategic incorporation of these non-metal dopants in NiS can facilitate tailored enhancements in its catalytic performance, making it more versatile for applications such as solar-driven water splitting and environmental pollutant degradation. These modifications impact the material's optical and electronic properties and play a crucial role in minimizing charge carrier recombination, ultimately optimizing the efficiency of NiS as a photocatalyst for sustainable energy and environmental applications.[45] Non-metal doping operates by introducing a new valence band above the original, narrowing the gap between the conduction and valence bands, as illustrated in Fig. 9.

For example, introducing doped S atoms or creating C and N-vacancies in g-C_3N_4 can broaden the light response range by either narrowing the band gap or generating gap states. Simultaneously, the coupling effect at the interface of g-C_3N_4/MoS_2 allows for tuning the band edge potentials of g-C_3N_4.[46]

So, the increasing interest in non-metal doping arises from the advantageous properties of high ionization energies and electronegativity, forming stable covalent bonds and enhanced thermal stability. Non-metal dopants, such as phosphorus, oxygen, nitrogen, boron, and carbon, induce diverse modifications in the semiconductor properties of NiS, crucially influencing its photocatalytic behavior. Nitrogen doping, in particular, widens the bandgap, boosting light absorption and

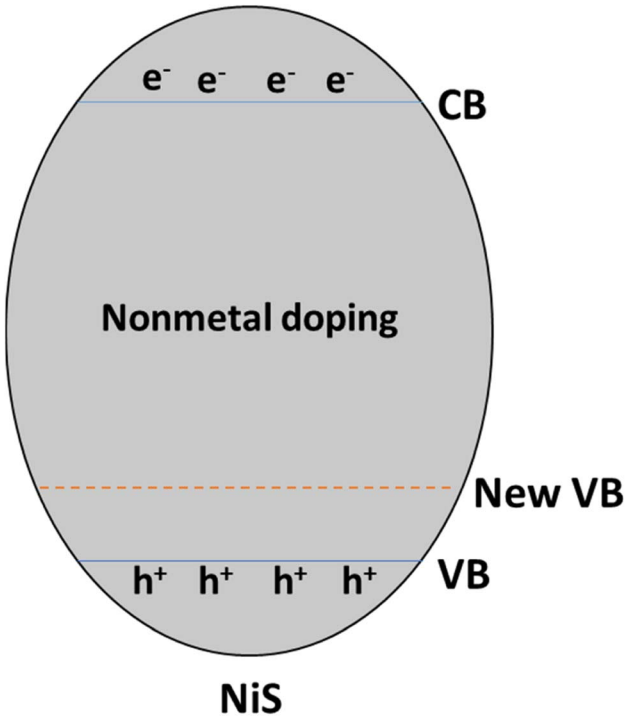

Fig. 9 Schematic illustration of the band structure modification due to non-metal doping.

catalytic activity. The strategic incorporation of these non-metal dopants allows tailored enhancements in NiS, optimizing its efficiency as a photocatalyst for sustainable energy and environmental applications. The band structure modifications due to non-metal doping illustrate the potential for expanding the light response range and tuning band edge potentials, further enhancing the versatility of these materials.

4.1.3 Halogen and metalloid doping. Metalloids are elements that exhibit properties of both metals and nonmetals. They have limited electrical conductivity and intermediate melting points. Halogens, such as fluorine and chlorine, are highly reactive elements found in group 17, which form diatomic molecules.[40]

For instance, Ni–Fe–P–B is a metalloid-doped catalyst that exhibits remarkable electrocatalytic activity and stability for the oxygen evolution reaction (OER) and hydrogen evolution reaction (HER). At low overpotentials of 220 mV and 269 mV, respectively, it can achieve a current density of 10 mA cm^{-2}. When the Ni–Fe–P–B@CFP electrode is integrated into carbon fiber paper (CFP) as a bifunctional catalyst, it exhibits effective overall water splitting at a low cell voltage of 1.58 V. For 60 h, it sustains a steady 10 mA cm^{-2} current density with very little deterioration. The remarkable catalytic efficacy of Ni–Fe–P–B is principally attributed to the modification of the combined metal–metalloid composition and its distinct amorphous structure.[47] Fig. 10 (ref. 47) illustrates the overall water-splitting performance of Ni–Fe–P–B@CFP.

Doping nickel sulfide (NiS) with halogens (*e.g.*, chlorine, fluorine) and metalloids (*e.g.*, silicon, phosphorus) significantly modifies its properties and enhances its photocatalytic activity

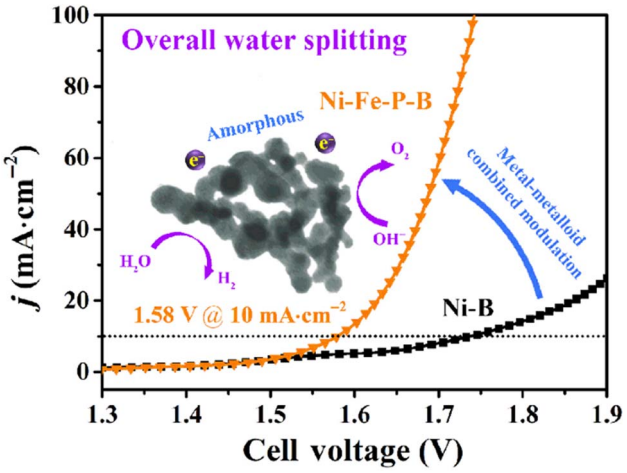

Fig. 10 The overall water-splitting performance of Ni–Fe–P–B@CFP.[47]

for dye degradation. Halogen doping modifies the electronic structure, while metalloid doping allows for bandgap engineering, optimizing light absorption and charge carrier dynamics.[48] Combining both dopants may synergistically impact factors like band structure and stability, which can lead to the design of efficient photocatalysts for environmental applications. The ultimate goal is to create photocatalysts that can effectively degrade dyes in an environmentally friendly way.[49]

Chemical doping, for instance, is a well-known technique for band gap engineering that modifies the electrical and surface properties of carbon nanomaterials by substituting foreign heteroatoms for carbon atoms. As effective chemical dopants for carbon nanomaterials, boron (B), phosphorus (P), and halogens such as fluorine (F), chlorine (Cl), bromine (Br), and iodine(I) are proposed. By producing an induced polarization network and positive/negative charges on neighboring carbon atoms, the differential in electronegativity between carbon and heteroatoms amplifies the oxygen reduction process (ORR). The doped carbons' optical, electrical, and magnetic characteristics are also influenced by this polarization network. By introducing different charge and spin densities to nearby carbon atoms, heteroatom doping produces surface active spots that effectively aid electron transport.[48]

So, the combination of metalloid and halogen doping in catalysts, such as Ni–Fe–P–B, demonstrates exceptional electrocatalytic activity and stability for the oxygen evolution reaction (OER) and the hydrogen evolution reaction (HER). This multifunctional catalyst, integrated into carbon fiber paper, achieves efficient overall water splitting at low cell voltages, sustaining a steady current density for an extended period. Furthermore, doping nickel sulfide (NiS) with halogens and metalloids enhances its photocatalytic activity for dye degradation by modifying the electronic structure and enabling bandgap engineering. The synergistic effects of combining these dopants offer promising prospects for designing efficient photocatalysts with improved band structure and stability for environmentally friendly dye degradation applications.

4.1.4 Co-doping. Co-doping is a technique commonly used in materials science and chemistry that involves simultaneously introducing two or more dopant elements into materials like semiconductors or catalysts for specific applications. Researchers use this technique to attain synergistic effects that enhance properties beyond what single-element doping achieves. Key aspects of co-doping include the fine-tuning of material properties, the precise control of characteristics through dopant concentration adjustments, and its applications in semiconductor technology and catalysis. Co-doping semiconductor materials, for example, can improve photocatalysis by optimizing visible light absorption and charge separation. However, co-doping strategies pose challenges, requiring careful consideration of dopant selection, concentrations, and their impact on material structure. Co-doping is a versatile tool for tailoring materials with enhanced or novel properties in electronics, energy storage, and catalysis.[50]

For instance, Co–NiS_2/CoS_2 exhibited exceptional catalytic performance in the hydrogen evolution reaction. The overpotential dramatically dropped to −133.3 mV when the Co (cobalt) doping content was increased to 27%. Compared to the non-doped case, where the overpotential was −214.3 mV, this indicates an 81 mV reduction.[51]

Similar to the findings in Mo, Co–NiO/NF, Mo, Co–NiS/NF-350 (Fig. 11a) showed a comparatively flat NF surface with small bulks (about 300 nm) evident (Fig. 11b and inset). Dense bulks ranging from 3 to 7 μm were seen on the NF surface in Mo, Co–NiS/NF-400 (Fig. 11c and d). The morphology of Mo, Co–NiS/NF-450 (Fig. 11e and f) was comparable to that of Mo, Co–NiS/NF-400, although it was smaller (about 10 μm) and had specific characteristics disturbed. Because of the low sulfurization temperature, a film-like substance with small bulks formed on the NF surface for Mo, Co–NiS/NF-350, indicating a lack of active sites for water splitting. Both the number and size of bulks grew as the temperature rose. However, the bulks shattered around 450 °C, leading to overly large sizes that impeded electron transport and active site exposure during water splitting. It was noted that HER and OER's electrochemical activity had decreased. The bulk morphology and unique fringe spacings (0.198 nm and 0.480 nm) that matched $Co_{0.5}NiS_2$ (102) and NiS (110), respectively, were revealed by the TEM and HRTEM images of Mo, Co–NiS/NF-400 (Fig. 11g and h). The HRTEM image showed a thin film of carbon wrapping around $Co_{0.5}NiS_2$, improving electrical contact and speeding up electron transmission. The uniform distribution of Co, Ni, Mo, S, C, and N elements in the SEM element mapping of Mo, Co–NiS/NF-400 (Fig. 11i) suggested that these components were converted from ZIF-67, which is consistent with the benefits of employing ZIF-67 as a precursor.[52]

Co-doping involves the simultaneous introduction of two or more dopant elements, a versatile technique in materials science with applications in semiconductors and catalysis. The precise control of material properties through dopant concentration adjustments allows for synergistic effects, as demonstrated by the outstanding electrocatalytic performance of Co–

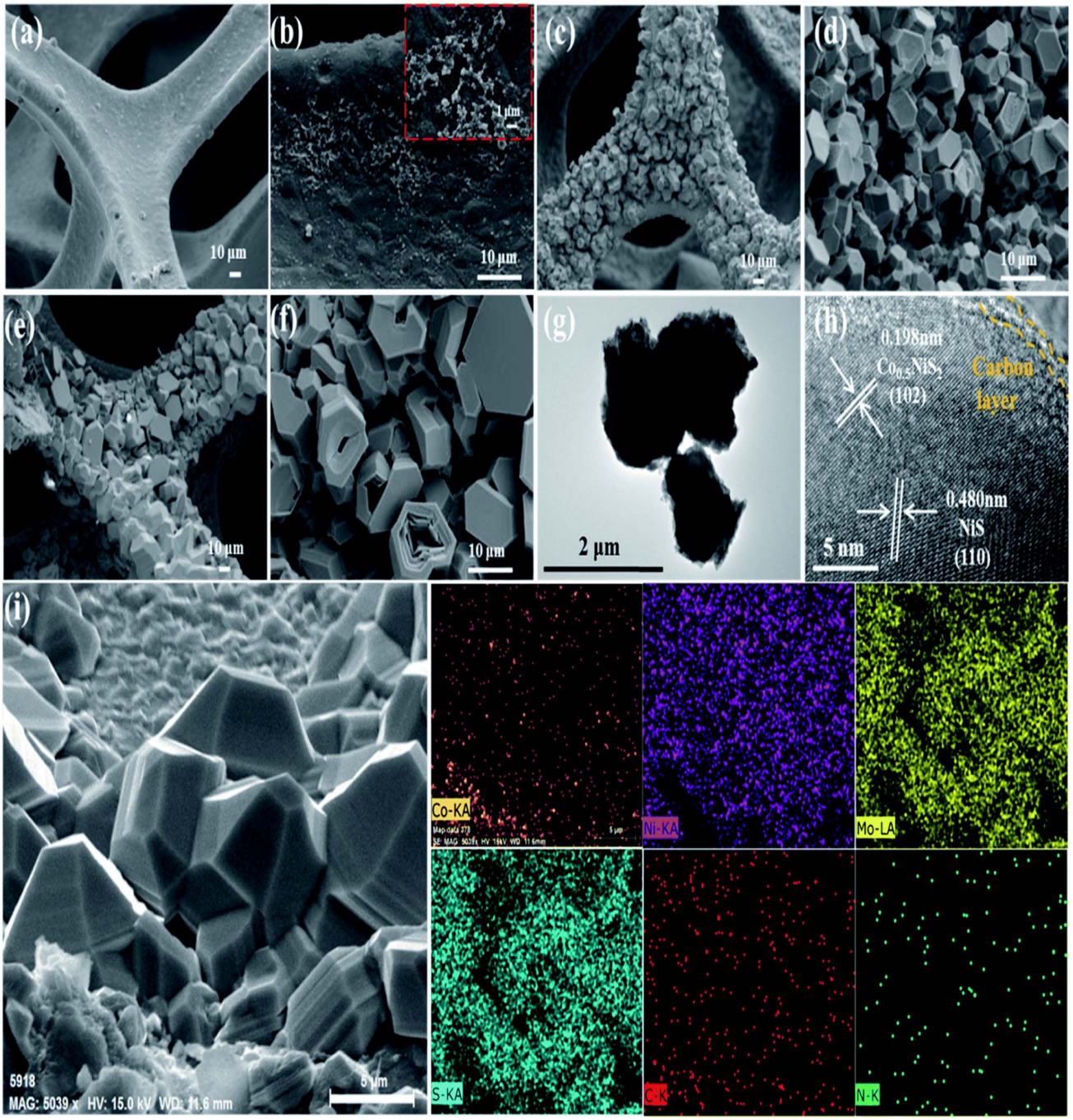

Fig. 11 (a and b) Mo, Co–NiS/NF-350, (c and d) Mo, Co–NiS/NF-400, and (e and f) Mo, Co–NiS/NF-450 are the synthesized materials' SEM pictures. Furthermore, bulks from Mo, Co–NiS/NF-400 are shown in (g) as TEM pictures, and bulks from the same sources are shown in (h) as HRTEM images. Lastly, (i) shows the Mo, Co–NiS/NF-400 EDS mapping image.[52]

NiS_2/CoS_2 in the hydrogen evolution reaction. The morphological and structural variations observed in Mo, Co–NiS/NF catalysts illustrate the temperature-dependent changes impacting electrochemical activity. Additionally, the formation of nickel sulfide composite powders with metal oxides through solution combustion synthesis reveals the significance of heating modes in determining material phases and properties, influencing photocatalytic degradation rates. Co-doping strategies offer promising avenues for tailoring materials with enhanced properties across various applications, including electronics, energy storage, and catalysis.

In conclusion, metals are usually shiny, malleable, and conductive elements. On the other hand, non-metals lack these properties and often exhibit various reactivity levels. Halogens refer to a group of highly reactive non-metals, while metalloids possess characteristics of both metals and non-metals. Doping

Table 2 Pros and Cons of the doping methods for fabrication of nickel sulfide

Doping type	Pros	Cons
Metal doping	• Enhances electrical conductivity • Improves mechanical properties • Introduces specific functionalities	• May introduce impurities affecting properties • Limited applicability due to crystal structure mismatch • Decreased material stability
Non-metal doping	• Enhances optical properties • Cost-effective compared to metal doping • Modifies electronic properties	• May introduce defects affecting the performance • Challenging to control doping concentration • Limited dopant solubility
Halogen/metalloid doping	• Offers tunability of material properties • Enables fine-tuning of band structures • Improves electronic and optical properties	• Potential for introducing deep-level effects • Requires careful processing conditions • Limited compatibility with certain host materials
Co-doping	• Synergistic effects • Greater control over properties • Mitigates drawbacks of single-element doping	• Increased complexity in doping processes • Challenges in achieving optimal doping ratios • Risk of dopant segregation or phase separation

is introducing impurities into a material to modify its properties, commonly done in semiconductors. Halogen or metalloid doping involves adding elements from these groups to modify material conductivity or reactivity, which is crucial in semiconductor manufacturing. Co-doping combines multiple dopants to fine-tune material properties synergistically, enhancing conductivity or other desired characteristics, which is pivotal in semiconductor research and electronics development. Each doping strategy has advantages and limitations, and the choice depends on the specific material requirements and desired application. The pros and cons of metal, non-metal, halogen/metalloid, and co-doping are outlined in Table 2.

4.2 Nanocomposite formation

4.2.1 With metal oxides. Solution combustion synthesis is used to prepare nickel sulfide composite powders with metal oxides. This process utilizes both conventional and microwave heating for ignition. Phases such α-NiS, NiS_2, Ni_3S_2, and NiO are generated depending on the ratio of urea and thiourea in the mixed fuel. The heating mode chosen plays a crucial role in determining the resulting phases and properties of the synthesized materials. In conventional heating mode, achieving an optimal combustion temperature and sulfur content in the precursor is possible. This requirement makes it easier to synthesize a sample with the most α-NiS phase, particularly when utilizing a fuel mixture with a urea-to-thiourea molar ratio of 2 : 1.75. On the other hand, NiO is formed, and sulfur-rich phases oxidize to sulfur-lean sulfide phases after microwave heating. The development of a bulky microstructure with larger sintered particles is caused by the raised combustion temperature during microwave heating. Because the powders burned using traditional methods had smaller particles, they were better at adsorbing substances. In contrast, the powders combusted through microwave heating achieved heightened photodegradation rates owing to their increased crystallinity.[8] Fig. 12a illustrates the photocatalytic degradation rates, while Fig. 12b displays the degradation kinetic curves of methylene orange (MO) when subjected to pure TiO_2 nanosheets arrays (NSAs) and *x*-NiS/TiO_2 p–n heterostructured NSAs with varying NiS content.[53]

So, solution combustion synthesis, employing both conventional and microwave heating, proves pivotal in tailoring nickel sulfide composites with metal oxides. The choice of heating mode influences the resulting phases, with traditional heating favoring α-NiS and microwave heating leading to NiO formation. The distinct microstructures produced under each method

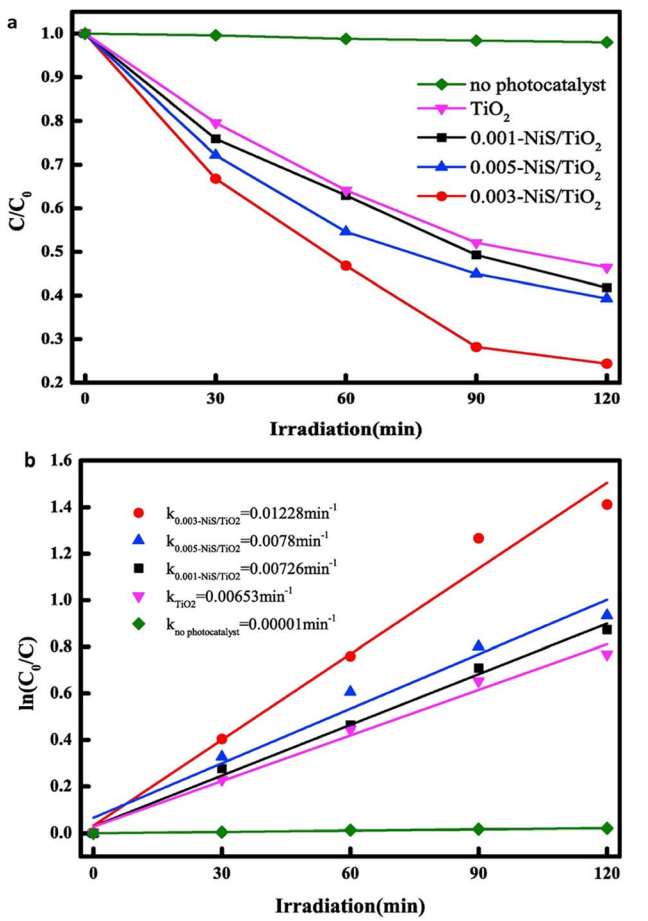

Fig. 12 (a)The degradation rates for photocatalysis and (b) the kinetic curves of methyl orange (MO) degradation for both pure TiO_2 nanosheets arrays (NSAs) and *x*-NiS/TiO_2 p–n heterostructured NSAs with varying NiS content.[53]

impact adsorption and photodegradation rates. Specifically, composites generated through microwave heating exhibit heightened photodegradation rates attributed to increased crystallinity. The presented figures highlight the photocatalytic degradation rates and kinetic curves, emphasizing the potential of *x*-NiS/TiO_2 p–n heterostructured nanosheet arrays for efficient degradation of methylene orange. These insights contribute to understanding synthesis techniques for tailored materials with enhanced photocatalytic properties.

4.2.2 With metal sulfides. Metal sulfates, especially those based on cadmium sulfide, are highly appreciated for their suitable energy band alignment and low band gap (~2.4 eV), which makes them useful for photodegradation reactions.[54] Unfortunately, low solar energy use and the quick recombination of photogenerated electron–hole pairs limit the efficiency of cadmium sulfide. The addition of more metals to create solid solutions is thought to be a workable solution to this problem.[55] By changing the metal ratio, this method enables accurate valence band (VB) and conduction band (CB) level modification.[56]

In a study conducted by Zhang *et al.*,[57] a flower-like 3NiS/$Zn_{0.5}Cd_{0.5}S$ composite catalyst is synthesized using a straightforward two-step method. Nickel sulfide (NiS) behaves as a co-catalyst, significantly improving the photocatalytic efficiency of $Zn_{0.5}Cd_{0.5}S$. The ultimate conversion efficiency of 3NiS/ZCS attains a remarkable 99.1% upon adding NiS, signifying a significant enhancement in both conversion rate and efficiency. Moreover, the catalyst demonstrates robust cycling stability, establishing itself as a reliable and promising photocatalyst with broad potential for industrial applications. This work underscores the significance of metal sulfide nanocomposites in overcoming limitations associated with conventional cadmium sulfide-based materials.

In Fig. 13a, the photocatalytic performance of CdS-T180 is depicted, revealing the influence of different concentrations of NiS loading on its efficacy. The graph provides valuable insights into how varying NiS content affects the overall performance of the photocatalytic system, shedding light on the optimal loading conditions for CdS-T180. Moving on to Fig. 13b, a comprehensive analysis of the photocatalytic activities of CdS-T_x samples is presented. This figure captures the performance of the samples both before and after the introduction of 1.5 wt% NiS loading. The comparison allows for a detailed examination of the impact of NiS dosage on the photocatalytic behavior of CdS-T_x, offering crucial information about the enhancement or alteration of the photocatalytic activities under the influence of NiS.

In conclusion, synthesizing a flower-like 3NiS/ZCS composite catalyst presents a promising strategy to enhance the efficiency of cadmium sulfide-based materials for photodegradation reactions. Incorporating nickel sulfide (NiS) as a co-catalyst results in a substantial improvement, achieving an impressive 99.1% conversion efficiency and demonstrating robust cycling stability. The study highlights the potential of metal sulfide nanocomposites in overcoming limitations associated with conventional cadmium sulfide, offering valuable insights into optimizing NiS loading conditions for enhanced photocatalytic performance. The depicted photocatalytic activities of CdS-T_x samples underscore the significance of carefully tuning NiS dosage for improved hydrogen production in the quest for efficient and stable photocatalysts.

4.2.3 With 2D layered materials. Nickel sulfide (NiS) composites, integrated with various 2D materials such as hydroxyapatite (HAP),[59] graphitic carbon nitride (g-C_3N_4),[60] biochar,[61] and thiosemicarbazide (SCN), have shown improved properties for diverse applications. The integration of NiS with HAP enhances biocompatibility while coupling it with g-C_3N_4

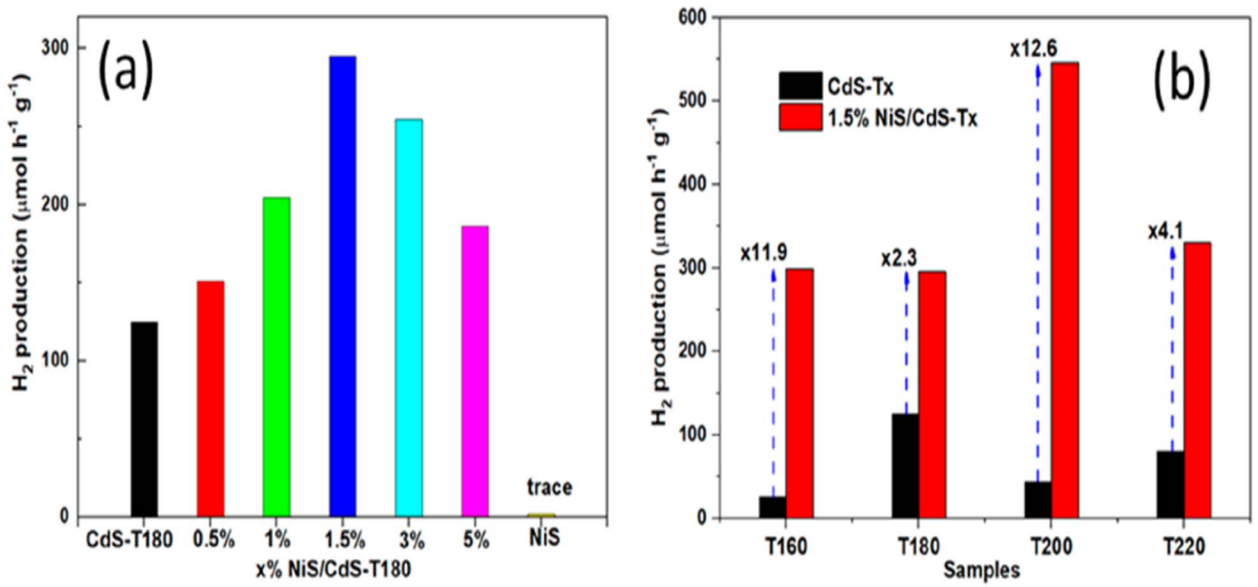

Fig. 13 (a) The photocatalytic efficacy of CdS-T180 with varying concentrations of NiS (b) photocatalytic activity of CdS-T_x samples before and after the addition of 1.5 wt% NiS for H_2 production.[58]

improves photocatalytic performance. The incorporation of biochar enhances stability and pollutant removal efficiency. Combining NiS with SCN improves electrocatalytic activity. These 2D material-NiS composites showcase versatile functionalities, making them promising candidates for a wide range of applications, from biomedicine to environmental remediation and energy conversion.[62] Fig. 14 (ref. 63) represents the photocatalytic performance of Co–NiS/g-C_3N_4.

Zhou *et al.*[64] introduced a facile one-pot hydrothermal method for synthesizing S-doped carbon nitride (CN) loaded with NiS nanoparticles. Compared to pure CN, the sulfur (S) doping improved charge carrier separation and transfer efficiency under visible light irradiation and increased light absorption. The combination of NiS with SCN further facilitated these processes. Consequently, S-doping and NiS loading significantly improved the photocatalytic activities of CN for RhB degradation and H_2 evolution. Optimal loading contents of S and NiS were identified for optimal photocatalytic performance. The SCN/NiS composite demonstrated outstanding photocatalytic activity and stability in RhB degradation and H_2 evolution. This method offers a straightforward approach to fabricating multifunctional, highly active modified carbon nitride photocatalysts for environmental remediation and energy catalysis applications.

So, the integration of nickel sulfide (NiS) with various 2D materials such as hydroxyapatite (HAP), graphitic carbon nitride (g-C_3N_4), biochar, and thiosemicarbazide (SCN) yields versatile composites with enhanced properties. These composites exhibit improved biocompatibility, photocatalytic performance, stability, and electrocatalytic activity. The Co–NiS/g-C_3N_4 nanocomposite, as depicted in Fig. 14, exemplifies enhanced photocatalytic performance.[63] Additionally, the one-pot hydrothermal synthesis of S-doped carbon nitride loaded with NiS nanoparticles demonstrates improved charge carrier dynamics, light absorption, and superior photocatalytic activities for Rhodamine B degradation and H_2 evolution. These findings underscore the potential of 2D material-NiS composites for diverse applications, ranging from environmental remediation to energy catalysis.

4.2.4 With 3D layered materials. Nickel sulfide (NiS) composites, which incorporate metal–organic frameworks (MOFs) and spinels, have distinctive properties when synthesized innovatively. Fig. 15a displays the UV-vis spectra, while Fig. 15b illustrates the Tauc plot, showcasing a comparison against bare MOF-5 and TMS@MOF-5. The study signifies the enhanced optical properties of MOF-5 when combined with NiS.

In a recent study, Wang *et al.*[12] synthesized a NiS/LFO heterostructured nano-photocatalyst using modified NiS nanosheets on LFO nanoparticles through a simple two-step hydrothermal method. The 5.0%-NiS/LFO system demonstrated superior photocatalytic activity for degrading methyl orange (MO), achieving a 90.9% removal rate in 120 min. The matched energy band and nanosheet structure of NiS contributed to enhanced light harvesting and efficient transfer of photogenerated carriers, leading to significantly improved photocatalytic performance. In a separate study, Nezamzadeh-Ejhieh *et al.*[66] synthesized NiS-incorporated zeolite P, demonstrating efficient degradation of E.B.T. dye under UV light. The results show the potential of NiS in zeolite structures for efficient dye decolorization. The ideal settings were pH 9.1, 0.8 g L^{-1} catalyst loading, and 40 ppm dye concentration.

Thus, the innovatively synthesized nickel sulfide (NiS) composites, incorporating metal–organic frameworks (MOFs) and spinels, exhibit distinctive properties, as illustrated by UV-vis spectra and Tauc plots in Fig. 15. Wang *et al.*'s study introduces a superior NiS/LFO heterostructured nano-photocatalyst, showcasing remarkable efficiency in degrading methyl orange. The matched energy band and nanosheet structure of NiS

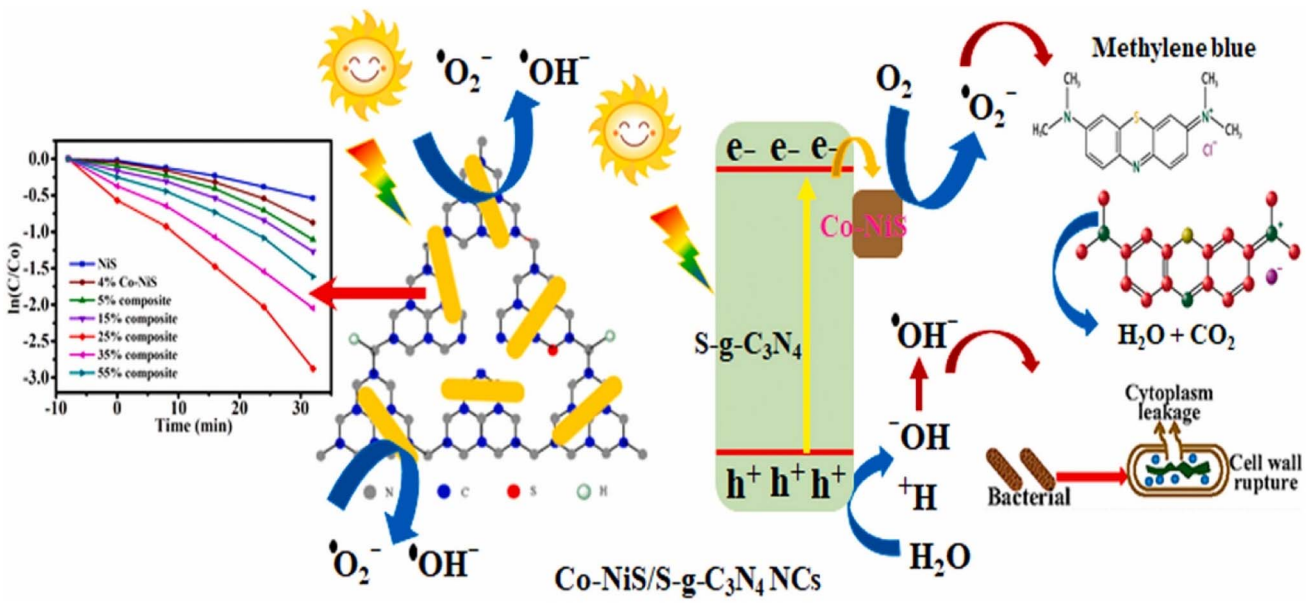

Fig. 14 Pictorial representation of the photocatalytic performance of Co–NiS/g-C_3N_4 nanocomposite.[63]

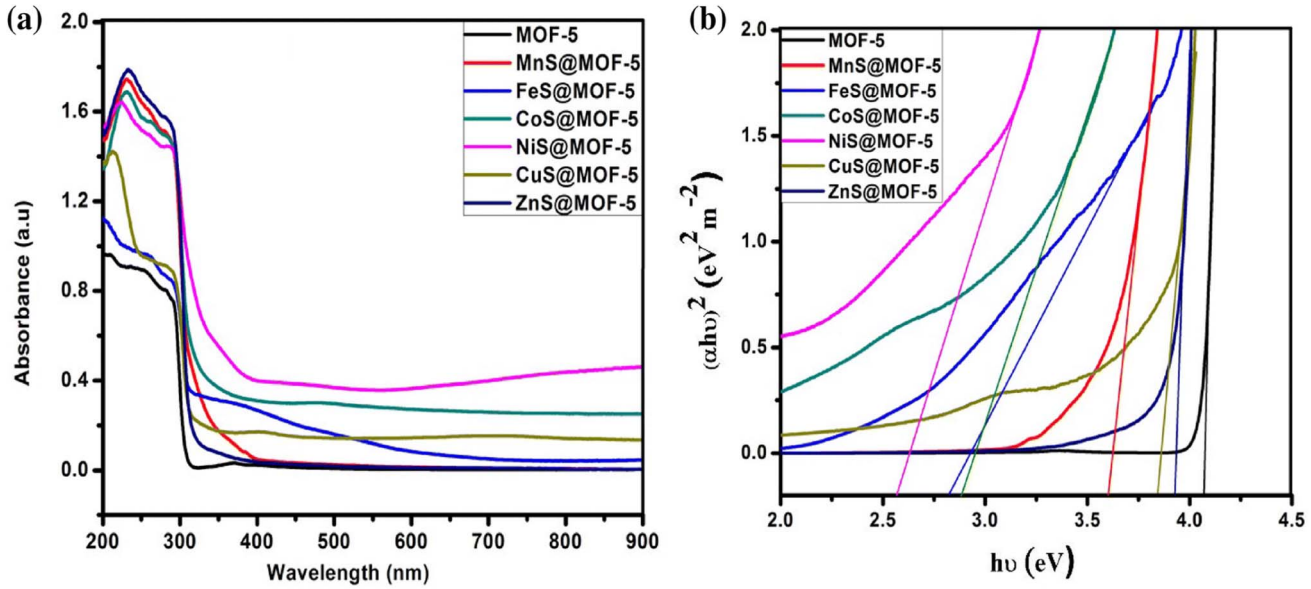

Fig. 15 (a) UV-vis spectrum (b) Tauc plot of bare MOF-5 and TMS@MO5.[65]

contribute to enhanced light harvesting and efficient carrier transfer, underlining its potential for advanced photocatalytic applications. Additionally, Ejhieih *et al.*'s work demonstrates the efficiency of NiS-incorporated zeolite P in degrading E.B.T. dye under UV light, highlighting the promising role of NiS in zeolite structures for effective dye decolorization under optimized conditions.

4.3 Surface area and morphology

The efficiency of chemical reactions largely depends on a photocatalyst's surface area. Researchers frequently utilize small particles dispersed in solvents or make porous films to improve the surface area. Because of their distinct physical characteristics in comparison to bulk materials, nanostructured materials with crystallite or grain sizes smaller than 20 nm are very fascinating. This creates new opportunities for applying photocatalysis in numerous domains.[62] The surface morphology of the photocatalyst, including the size of particles and agglomerates, plays a significant role in the photocatalytic degradation process. The interaction between organic molecules and the photocatalyst surface coverage directly affects the reaction rate, which is controlled by the number of photons that strike the

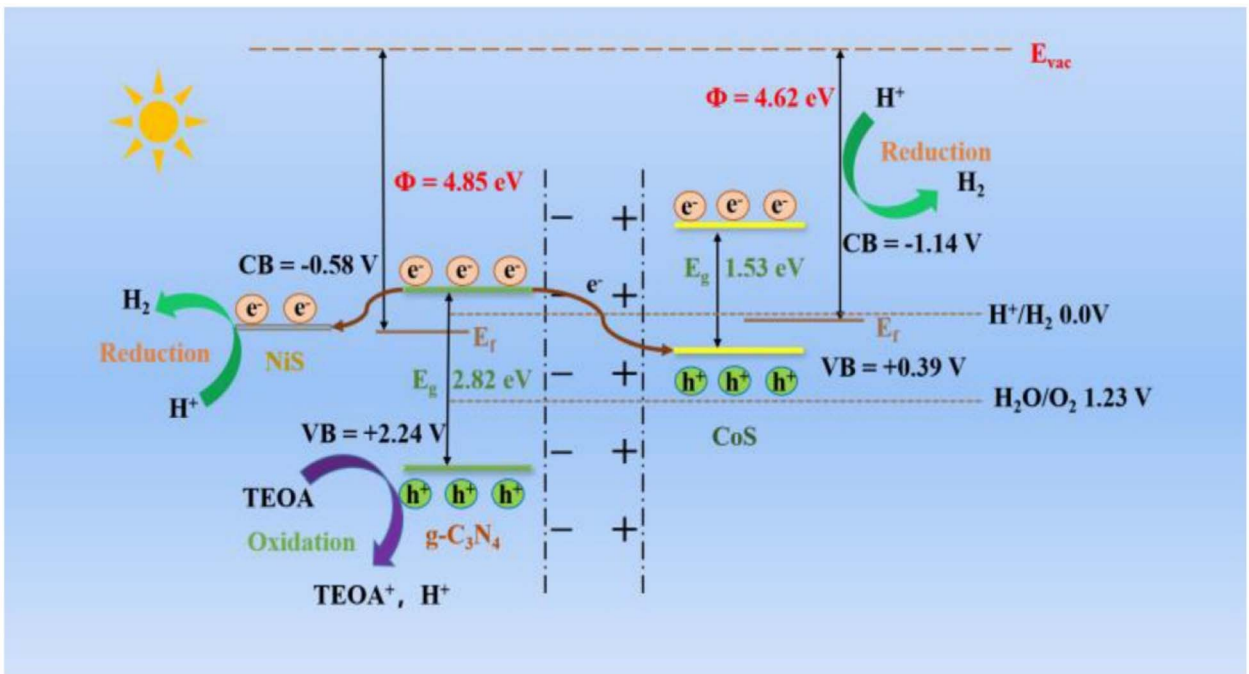

Fig. 16 The band structure and hydrogen evolution mechanism of CoS/CN/NiS composites are under consideration.[67]

photocatalyst. Defect-rich morphologies are generally associated with increased photocatalytic activity.[10]

As an example, the improved photocatalytic performance observed in $NiS/MoS_2/g\text{-}C_3N_4$ hybrids was attributed to several factors, including increased surface adsorption, enhanced light absorption, and more efficient charge separation and transfer.[67] The proposed mechanism for electron–hole separation and transport in these ternary $NiS/MoS_2/g\text{-}C_3N_4$ hybrids under visible light irradiation is illustrated in Fig. 16.[67]

Thus, the efficiency of chemical reactions in photocatalysis is closely tied to the surface area of the photocatalyst, with nanostructured materials offering unique opportunities due to their distinct physical characteristics. The surface morphology, including particle size and agglomerates, significantly influences the photocatalytic degradation process, with defect-rich morphologies generally associated with increased activity. In the case of $NiS/MoS_2/g\text{-}C_3N_4$ hybrids, the enhanced photocatalytic performance is attributed to factors such as improved surface adsorption, enhanced light absorption, and more efficient charge separation and transfer, as illustrated in the proposed mechanism in Fig. 16. These insights underscore the importance of tailored nanostructures in optimizing photocatalytic processes for various applications.

5. Recent advancements in NiS-based nanocomposites

The increasing need for effective and sustainable energy technologies has led to a notable upsurge in NiS nanocomposite-related research and development in recent years. These nanocomposites, which usually consist of different materials mixed with nickel sulfide (NiS), have attracted interest due to their excellent qualities and potential uses in energy storage and conversion systems. The requirement for NiS nanocomposites stems from the necessity to enhance advances in renewable energy technology while addressing the issues related to traditional energy sources. Because of its distinct electrical and catalytic characteristics, NiS is a viable option for improving the efficiency of energy-related equipment. Improved surface reactivity, optimized electrocatalytic activity, and improved charge transport are made possible by the synergistic effects of nanocomposite engineering. These developments find use in various industries, including batteries, solar cells, and electrocatalytic systems for hydrogen evolution. The search for NiS nanocomposites underscores their critical role in influencing the direction of next-generation energy technology and is a calculated reaction to the worldwide need for clean and sustainable energy solutions. The investigations conducted to investigate and analyze the characteristics and uses of these nanocomposites are detailed in Table 3.

The study by Khosravi *et al.*[14] led to the synthesis of nickel sulfide nanoparticles in an eco-friendly manner using a hydrothermal process. An innovative sulfur source, 1-benzylidene thiosemicarbazide, was used along with nickel sulfide to create the nanoparticles. The resulting cauliflower-like structures showed a blue shift in the band gap, attributed to the disciplined arrays and small dimensions of the nanoparticles, and had a smaller band gap than the bulk material. This resulted in an enhanced efficiency. In another work, nickel sulfide (NiS) nanoflowers have been successfully synthesized using a simple polyol refluxing method at room temperature. The thickness of these nanoflowers ranges from 5 to 10 nm, while their size can reach several hundred nm. The photocatalytic efficiency of these NiS nanoflowers has been evaluated and found to be excellent. After 3 h of exposure to visible light, the decomposition rate of methylene blue (MB) reached nearly 98%. This finding highlights the potential of NiS nanoflowers as high-performance photocatalysts. The band structure analysis has revealed that charge transfer occurs from the S 3p orbital to the unoccupied Ni orbital during photoexcitation.[22]

Soofivand *et al.*[68] successfully synthesized nickel sulfide (NiS_2) nanostructures by employing a simple hydrothermal process and a novel nickel source. The reaction of an organometallic precursor achieved the formation of these nanostructures, $[Ni(pht)(H_2O)_2]$, with several sources of sulfur, such as thiourea, CS_2, $(NH4)_2S$, and cysteine. The final product's band gap of around 2.2 eV has verified that it is a semiconductor. The fact that the measured band gap was more significant than that of bulk NiS_2 was fascinating, perhaps because of the quantum effects present in nanomaterials. Furthermore, nickel sulfide (NiS) nanoparticles were successfully synthesized by Fazil *et al.*[33] using an economical, low-temperature chemical method that didn't require templates. They optimized the chemical precipitation process by employing Taguchi's robust route to achieve nickel sulfide nanoparticles with the smallest size and consistent morphology.

Ardebilchi Marand *et al.*[8] produced nickel sulfide composite powders by solution combustion with mixed urea–thiourea fuels in different proportions, with nickel nitrate acting as an oxidant and source of nickel. The greater combustion temperature in the microwave heating process led to the oxidation of the sulfide phase to nickel oxide. The most NiS phase was produced by the traditional synthesis method, which had a urea-to-thiourea molar ratio of 2 : 0.75 and a maximum methylene blue (MB) elimination effectiveness of about 52%. In another research work, a new photocatalyst called $NiS/BiVO_4$, which is a p–n heterostructure, has been developed by Li *et al.*[11] Integrating p-type NiS nanoparticles with n-type decahedral nanostructured $BiVO_4$ results in improved light absorption, boosted photocurrent response, and effective photo-generated electron–hole pair separation and transfer.

In a study, Arumugam *et al.*[6] successfully created a heterojunction photocatalyst by synthesizing NiS/rGO using a one-step hydrothermal process. This method enabled a close interaction between NiS and rGO, enabling the quick transition of photogenerated electrons from rGO to NiS. Consequently, the recombination of charged particles was reduced, which improved photocatalytic efficiency.

Furthermore, in a study, Wang *et al.*[12] used a straightforward two-step hydrothermal process to generate a unique $NiS/LaFeO_3$ heterostructure with the morphology of $LaFeO_3$ nanoparticles fixed NiS nanosheets. Extensive experiments show that the enhanced photocatalytic performance of $NiS/LaFO_3$ is

Table 3 Recent developments in NiS-based catalysts for photocatalytic contaminant degradation

Nanocomposite	Synthesize method	Pollutants	Source of light	Catalyst dose ($g\ L^{-1}$)	Pollutant concentration ($g\ L^{-1}$)	Time (min)	Efficiency (%)	Ref.
NiS	Hydrothermal	Acid red Acid brown Methyl red Methyl orange Methylene blue	UV light	0.4	0.01	150	90 96 85 81 72	14
NiS	Polyol refluxing	Methylene blue Rhodamine B	500 W xenon lamp	1	0.008	180	98 75	22
NiS_2	Hydrothermal	Erythrosine Phenol red	UV light	0.02	0.02	75	57 71	68
Ni_3S_2 and NiS	Chemical precipitation, optimized by Taguchi robust route	Methylene blue	250 W UV lamp	0.04	0.05	160	98.5	33
Ni_xS_y/NiO	Solution combustion	Methylene blue	100 W xenon lamp	0.35	0.005	300	28	8
NiS/$BiVO_4$	Hydrothermal	Methyl orange	300 W xenon lamp	0.001	0.01	90	95.6	11
NiS/rGO	Modified Hummer's Method	Methylene blue	Sun light	10	0.03	100	95	6
NiS/$LaFeO_3$	Hydrothermal	Methyl orange	Sun light	0.005	0.02	120	90.9	12
NiS/CdS	Hydrothermal	Quinoline	500 W xenon lamp	0.002	0.05	600	68.2	23
NiS/TiO_2	Sol–gel	Sunset yellow	Sun light	4	3×10^{-4} M	80	98.9	1
NiS/TiO_2	Hydrothermal	Methyl orange	500 W xenon lamp	0.001	0.01	20	98	24
ZnS–NiS	Precipitation	2-Nitro toluene	55 W medium Pressure Hg lamp (Philips)	0.75	0.055	160	63	69
3NiS/$Zn_{0.5}Cd_{0.5}S$	Co-precipitation/solution impregnation	Methylene blue	300 W xenon lamp	2.5	0.012	120	99.1	57
NiS/Ag_2MoO_4	Precipitation	Methylene blue	55 W halogen-Tungsten lamp	0.3	0.01	140	91	70
NiS_2/rGO	Hydrothermal	Congo red	Sunlight (680 W m^{-2})	0.3	10	40	97.03	3
NiS/Zeolite	Precipitation	Erichrome black T	75 W Hg lamp	0.8	0.02	120	78	66
SCN/NiS	Hydrothermal	Rhodamine B	10 W LED lamp	—	—	15	71.6	64
α-Ag_2WO_4/NiS_x	Hydrothermal	Lomefloxacin	Visible light	—	—	60	98.4	71
$BiVO_4$/NiS/Au	Hydrothermal	Tetracycline	300 W xenon lamp	2	0.03	25	82	72
Cu–NiS/ZnS	Precipitation	Methyl green Methylene blue Congo red	Sunlight	0.5	0.02	60	98 92 85	38
ZnS–NiS/Zeolite	—	Metronidazole	35 W moderate Pressure Hg lamp	3	0.004	150	96.41	73
SGCN/Te@NiS	Hydrothermal	Methylene blue	Sunlight	2	2	70	97	39
β-$Ni(OH)_2$/NiS/TiO_2	Precipitation	Methyl orange	500 W Xe lamp	1	0.01	15	98	74
Ce_2S_3/NiS_2/rGO	Hydrothermal	Methyl orange Bromophenol blue	Sunlight	0.6	0.02	120	89.1 84.2	75
NiS_2/TiO_2/Cu	Microwave irradiation	Rhodamine B Methyl orange Acid brown Acid black	Visible light	0.005	0.005	120	92 86 87 88	76
FTO/$BiVO_4$/NiS	Hydrothermal	Rhodamine B	Sunlight	—	0.01	120	73	77

Table 3 (*Contd.*)

Nanocomposite	Synthesize method	Pollutants	Source of light	Catalyst dose ($g\ L^{-1}$)	Pollutant concentration ($g\ L^{-1}$)	Time (min)	Efficiency (%)	Ref.
$CoNiO_2$–$BiFeO_3$–NiS	Precipitation	Methyl orange	500 W halogen lamp	—	—	160	99.8	78
		Rhodamine B				100	97.8	
g-C_3N_4/$MnWO_4$/NiS	Hydrothermal	Methylene blue	200 W LED lamp	—	—	150	91.6	79
NiS–Mg/S-BC	One-pot sulfurization	Rhodamine B	Sunlight	0.4	—	120	96.98	41
S-scheme NiS@ZrO_2	Facile impregnation	Ciprofloxacin	300 W xenon lamp	1	0.01	45	99.3	13

attributed to the matched energy band of NiS and $LaFeO_3$, which permits better interfacial electron separation and transfer, and the nanosheet structure of NiS, which allows photogenerated electrons to be transported without obstruction.

In another study, Wu *et al.*[23] produced NiS/CdS nanocomposites using microwave or hydrothermal techniques. When exposed to visible light, the resultant NiS/CdS nanocomposites demonstrated strong photocatalytic activity in the destruction of quinoline. This is because a p-NiS/n-CdS-m heterojunction forms a catalyst to lower electron–hole pair recombination and provides remarkable photocatalytic characteristics and high quantum efficiency. Moreover, $BiVO_4$, NiS, and Au ternary-nanocomposites were manufactured using a simple two-step approach, including hydrothermal treatment and photo-reduction. When compared to pure $BiVO_4$ photocatalysts or binary combinations like $BiVO_4$/NiS or $BiVO_4$/Au, the prepared $BiVO_4$/NiS/Au composites exhibit a remarkable enhancement in the degradation of organic pollutants. This is because the method uses Au's electron-collecting properties to form a p to n junction between NiS and $BiVO_4$. Interestingly, compared to pure $BiVO_4$, the ideal ternary $BiVO_4$/NiS/Au composites had a 4.25-fold greater photodegradation efficiency for tetracycline (TC).[72]

So, the extensive research on NiS nanocomposites reveals their significant potential in various applications, particularly in energy storage, conversion systems, and environmental remediation. The innovative synthesis methods, such as hydrothermal processes, polyol refluxing, and solution combustion, enable the production of diverse NiS nanomaterials with enhanced properties. These nanocomposites exhibit remarkable photocatalytic activities, improved charge transport, and optimized electrocatalytic performance. The studies highlight the crucial role of NiS nanocomposites in advancing clean and sustainable energy technologies. Future work may further optimize synthesis techniques, explore novel nanocomposite combinations, and scale up production for practical applications in diverse industries.

6. Future prospects

Due to their effective light-harvesting capabilities and exceptional photocatalytic activities—particularly in the area of dye degradation—nickel sulfide has gained popularity. The necessity of choosing an appropriate photocatalyst depending on the pollutant present in the application is highlighted by the fact that the usefulness of these catalysts is contingent upon the operational parameters. The instability of nickel sulfide nanoparticles, which can lead to agglomeration and decreased efficacy, is one of their problems.[80] Researchers have created creative solutions to this issue and improved the stability and effectiveness of nickel sulfide photocatalysts. Among these approaches, heterojunction generation and doping techniques have demonstrated the potential to mitigate the inherent drawbacks of pure nickel sulfide.[64] Recent research aims to develop innovative photocatalysts based on nickel sulfide with distinct properties such as high reusability, low electron–hole recombination rates, and more extensive surface areas. These

elements are essential for maximizing the overall performance of photocatalytic materials. For photocatalytic stability to be achieved and maintained, it is crucial to manipulate the crystallite's size, shape, and surface area. Despite advancements in improving nickel sulfide photocatalysts' characteristics, several obstacles still exist. One major drawback is the possibility of photo corrosion, which could cause the metal to ionize in the water sample. To lessen the likelihood of secondary pollution, more research is needed to determine whether metal ions are seeping into the water supply. In an effort to improve the long-term practical application of nickel sulfide-based photocatalysts, researchers are actively investigating the creation of stable heterojunctions that successfully avoid photo corrosion.[64] The surface area and adsorption efficiency of nickel sulfide control their photocatalytic activity. Scientists are investigating novel manufacturing methods to generate metal sulfide photocatalysts with increased surface areas. Adding nickel sulfide to fly ash or charcoal may be an excellent way to increase surface area and boost photocatalytic efficiency.[81] This is a subject that needs more research. Specific contaminants—especially artificial dye solutions—are the main focus of the investigation. However, since industrial wastewater usually contains a variety of contaminants, it's critical to comprehend how nickel sulfide functions as photocatalyst when combined with different dyes. In order to employ nickel sulfide-based photocatalysts efficiently for wastewater treatment, more investigation into the various natures of contaminants in industrial wastewater is required. Actual wastewater samples must be used instead of fake dye solutions to commercialize photocatalytic processes. Beyond colors, industrial wastewater is complicated and comprises a wide range of organic and inorganic pollutants, creating new problems that must be solved. Thorough testing using actual wastewater samples is necessary to confirm that photocatalysts based on nickel sulfide are effective in real-world settings.[82] The issue of stable heterojunctions and surface area improvement is still a top concern despite tremendous advancements in the industry. To produce these catalysts, researchers examine synthesis methods and consider variables like solvent selection, calcination temperature, and other parameters. The reusability and durability of photocatalyst materials are interdependent properties that impact overall photocatalytic performance and are carefully studied. To expand the applications, significant research is required to fabricate nickel sulfide-based photocatalysts with improved structural properties, photostability, reusability, and efficient regeneration. Beyond the breakdown of a single contaminant, the investigation of nanocomposites with enhanced capabilities for water remediation is a focal point.

Nickel sulfide exhibits remarkable photocatalytic activities, particularly in dye degradation, but faces challenges such as instability and agglomeration.[33] Researchers actively address these issues through innovative approaches like heterojunction generation and doping techniques to enhance stability and effectiveness. The focus is on developing photocatalysts with high reusability, low electron–hole recombination rates, and increased surface areas, essential for optimal performance. However, challenges like photo corrosion and the need for broader applicability to diverse industrial wastewater contaminants necessitate continued research to refine structural properties, photostability, and regeneration processes for nickel sulfide-based photocatalysts.

7. Conclusion

The exceptional visible light photocatalytic activity of nickel sulfide depends on the surface area, bandgap, and surface shape of the produced composite. However, their utility is severely limited by their charge recombination rates and stability. In order to get beyond these restrictions, scientists are investigating doping strategies and heterojunction production. New developments in synthesis methods have made it possible to create a variety of nanocomposites with improved water remediation capabilities. As research advances, it is critical to comprehend how variables like dopant concentration and shape affect the photocatalytic activity of nickel sulfide. Furthermore, the formation of nanocomposites and heterojunctions has steered the research in this field in a positive direction. The effective commercialization of nickel sulfide-based photocatalysts in various water treatment applications will depend on resolving these issues and deepening our understanding of these catalysts.

Conflicts of interest

There are no conflicts to declare.

References

1 D. Rajamanickam, P. Dhatshanamurthi and M. Shanthi, Enhanced photocatalytic efficiency of NiS/TiO_2 composite catalysts using sunset yellow, an azo dye under day light illumination, *Mater. Res. Bull.*, 2015, **61**, 439–447, DOI: 10.1016/J.MATERRESBULL.2014.09.095.

2 S. Muninathan and S. Arumugam, Enhanced photocatalytic activities of NiS decorated reduced graphene oxide for hydrogen production and toxic dye degradation under visible light irradiation, *Int. J. Hydrogen Energy*, 2021, **46**, 6532–6546, DOI: 10.1016/J.IJHYDENE.2020.11.178.

3 P. Borthakur and M. R. Das, Hydrothermal assisted decoration of NiS_2 and CoS nanoparticles on the reduced graphene oxide nanosheets for sunlight driven photocatalytic degradation of azo dye: effect of background electrolyte and surface charge, *J. Colloid Interface Sci.*, 2018, **516**, 342–354, DOI: 10.1016/J.JCIS.2018.01.050.

4 F. Torki and H. Faghihian, Photocatalytic activity of NiS, NiO and coupled NiS–NiO for degradation of pharmaceutical pollutant cephalexin under visible light, *RSC Adv.*, 2017, **7**, 54651–54661, DOI: 10.1039/C7RA09461B.

5 J. Fenoll, I. Garrido, P. Hellín, P. Flores and S. Navarro, Photodegradation of neonicotinoid insecticides in water by semiconductor oxides, *Environ. Sci. Pollut. Res.*, 2015, **22**, 15055–15066, DOI: 10.1007/S11356-015-4721-2/FIGURES/4.

6 P. Arumugam, P. Sengodan, N. Duraisamy, R. Rajendran and V. Vasudevan, An effective strategy to enhance the

photocatalytic performance by forming NiS/rGO heterojunction nanocomposites, *Ionics*, 2020, **26**, 4201–4212, DOI: 10.1007/S11581-020-03564-Y/FIGURES/15.

7 M. Ahmaruzzaman and S. R. Mishra, Photocatalytic performance of g-C_3N_4 based nanocomposites for effective degradation/removal of dyes from water and wastewater, *Mater. Res. Bull.*, 2021, **143**, 111417, DOI: 10.1016/J.MATERRESBULL.2021.111417.

8 N. Ardebilchi Marand, S. M. Masoudpanah, M. S. Bafghi and S. Alamolhoda, Photocatalytic activity of nickel sulfide composite powders synthesized by solution combustion method, *J. Electron. Mater.*, 2020, **49**, 1266–1272, DOI: 10.1007/S11664-019-07744-Z/METRICS.

9 S. R. Mishra and M. Ahmaruzzaman, Microplastics: identification, toxicity and their remediation from aqueous streams, *Sep. Purif. Rev.*, 2023, **52**, 283–304, DOI: 10.1080/15422119.2022.2096071.

10 V. Gadore, S. R. Mishra and M. Ahmaruzzaman, Metal sulphides and their heterojunctions for photocatalytic degradation of organic dyes-A comprehensive review, *Environ. Sci. Pollut. Res.*, 2023, **1**, 1–48, DOI: 10.1007/S11356-023-28753-W.

11 Y. Li, X. Li, X. T. Wang, L. J. Jian, N. I. M. Abdallah, X. F. Dong and C. W. Wang, p–n Heterostructured design of decahedral NiS/$BiVO_4$ with efficient charge separation for enhanced photodegradation of organic dyes, *Colloids Surf., A*, 2021, **608**, 125565, DOI: 10.1016/J.COLSURFA.2020.125565.

12 X. T. Wang, Y. Li, X. Q. Zhang, J. F. Li, X. Li and C. W. Wang, Design and fabrication of NiS/$LaFeO_3$ heterostructures for high efficient photodegradation of organic dyes, *Appl. Surf. Sci.*, 2020, **504**, 144363, DOI: 10.1016/J.APSUSC.2019.144363.

13 H. El-Hosainy, W. T. Alsaggaf, Z. I. Zaki and M. H. H. Mahmoud, Facile synthesis of S-scheme NiS@ZrO_2 nano-heterostructure for superior degradation of antibiotic under visible light irradiation, *Opt. Mater.*, 2022, **133**, 113011, DOI: 10.1016/J.OPTMAT.2022.113011.

14 M. Khosravi, S. Saeednia, P. Iranmanesh and M. Hatefi Ardakani, Cauliflower-like nickel sulfide nanostructures: preparation, optical properties, catalytic and photocatalytic activities, *J. Clust. Sci.*, 2023, **34**, 311–322, DOI: 10.1007/S10876-021-02210-5/TABLES/2.

15 R. Pothu, R. Bolagam, Q. H. Wang, W. Ni, J. F. Cai, X. X. Peng, Y. Z. Feng and J. M. Ma, Nickel sulfide-based energy storage materials for high-performance electrochemical capacitors, *Rare Met.*, 2021, **40**, 353–373, DOI: 10.1007/S12598-020-01470-W/FIGURES/9.

16 Y. Liu, D. Huang, M. Cheng, Z. Liu, C. Lai, C. Zhang, C. Zhou, W. Xiong, L. Qin, B. Shao and Q. Liang, Metal sulfide/MOF-based composites as visible-light-driven photocatalysts for enhanced hydrogen production from water splitting, *Coord. Chem. Rev.*, 2020, **409**, 213220, DOI: 10.1016/J.CCR.2020.213220.

17 Y. Xu and R. Xu, Nickel-based cocatalysts for photocatalytic hydrogen production, *Appl. Surf. Sci.*, 2015, **351**, 779–793, DOI: 10.1016/J.APSUSC.2015.05.171.

18 S. Begum, S. R. Mishra and M. Ahmaruzzaman, Fabrication of ZnO–SnO_2 nanocomposite and its photocatalytic activity for enhanced degradation of Biebrich scarlet, *Environ. Sci. Pollut. Res.*, 2022, **2022**, 1–14, DOI: 10.1007/S11356-022-21851-1.

19 A. Sharma, P. R. Makgwane, E. Lichtfouse, N. Kumar, A. H. Bandegharaei and M. Tahir, Recent advances in synthesis, structural properties, and regulation of nickel sulfide-based heterostructures for environmental water remediation: an insight review, *Environ. Sci. Pollut. Res.*, 2023, **30**, 64932–64948, DOI: 10.1007/S11356-023-27093-Z.

20 S. Chandrasekaran, L. Yao, L. Deng, C. Bowen, Y. Zhang, S. Chen, Z. Lin, F. Peng and P. Zhang, Recent advances in metal sulfides: from controlled fabrication to electrocatalytic, photocatalytic and photoelectrochemical water splitting and beyond, *Chem. Soc. Rev.*, 2019, **48**, 4178–4280, DOI: 10.1039/C8CS00664D.

21 J. Wang, S. Y. Chew, D. Wexler, G. X. Wang, S. H. Ng, S. Zhong and H. K. Liu, Nanostructured nickel sulfide synthesized *via* a polyol route as a cathode material for the rechargeable lithium battery, *Electrochem. Commun.*, 2007, **9**, 1877–1880, DOI: 10.1016/J.ELECOM.2007.04.020.

22 J. Chao, D. Duan, S. Xing, Y. Zhao, X. Zhang, S. Gao, X. Li, Q. Fan and J. Yang, Visible-light-driven photocatalytic properties and electronic structures of nickel sulfide nanoflowers, *Solid State Sci.*, 2015, **43**, 59–62, DOI: 10.1016/J.SOLIDSTATESCIENCES.2015.03.022.

23 D. Wu, F. Wang, Y. Tan and C. Li, Facile synthesis of NiS/CdS nanocomposites for photocatalytic degradation of quinoline under visible-light irradiation, *RSC Adv.*, 2016, **6**, 73522–73526, DOI: 10.1039/C6RA13439D.

24 Y. N. Luo, Y. Li, L. Long Qian, X. T. Wang, J. Wang and C. W. Wang, Excellent photocatalytic performance from NiS decorated TiO_2 nanoflowers with exposed {001} facets, *Mater. Res. Bull.*, 2020, **130**, 110945, DOI: 10.1016/J.MATERRESBULL.2020.110945.

25 S. L. Lee and C. J. Chang, Recent progress on metal sulfide composite nanomaterials for photocatalytic hydrogen production, *Catalysis*, 2019, **9**, 457, DOI: 10.3390/CATAL9050457.

26 H. Hafdi, J. Mouldar, M. Joudi, B. Hatimi, H. Nasrellah, M. A. El Mhammedi and M. Bakasse, Nickel sulfide impregnated on natural phosphate: characterization and applications in photocatalytic degradation of indigocarmine dye, *Opt. Quantum Electron.*, 2021, **53**, 1–13, DOI: 10.1007/S11082-021-02811-4/TABLES/1.

27 L. Zhu, Z. Da Meng, T. Ghosh and W. C. Oh, Enhanced photocatalytic efficiency of nanoscale NiS_2/TiO_2 catalysts synthesized by hydrothermal and sol-gel method, *J. Korean Ceram. Soc.*, 2012, **49**, 135–141, DOI: 10.4191/KCERS.2012.49.2.135.

28 C. A. Pandey, S. Ravuri, R. Ramachandran, R. Santhosh, S. Ghosh, S. R. Sitaraman and A. N. Grace, Synthesis of NiS–Graphene nanocomposites and its electrochemical performance for supercapacitors, *Int. J. Nanosci. Nanotechnol.*, 2017, **17**, 1760021, DOI: 10.1142/S0219581X17600213.

29 G. Suganya and G. Kalpana, Investigation of graphene based NiS nanocomposite by solvothermal method for energy

storage application, *Mater. Lett. X*, 2021, **12**, 100112, DOI: 10.1016/J.MLBLUX.2021.100112.

30 S. Kokilavani, A. Syed, L. L. Raju, S. Al-Rashed, A. M. Elgorban, A. M. Thomas and S. S. Khan, Synthesis of novel heterostructured FeS_2/Ag_2MoO_4 nanocomposite: characterization, efficient antibacterial and enhanced visible light driven photocatalytic activity, *Surf. Interfaces*, 2021, **23**, 101003, DOI: 10.1016/J.SURFIN.2021.101003.

31 Q. Chen, W. Chen, J. Ye, Z. Wang and J. Y. Lee, l-Cysteine-assisted hydrothermal synthesis of nickel disulfide/graphene composite with enhanced electrochemical performance for reversible lithium storage, *J. Power Sources*, 2015, **294**, 51–58, DOI: 10.1016/J.JPOWSOUR.2015.06.071.

32 H. Liu, Z. Liu, F. Wang and L. Feng, Efficient catalysis of N doped NiS/NiS_2 heterogeneous structure, *Chem. Eng. J.*, 2020, **397**, 125507, DOI: 10.1016/J.CEJ.2020.125507.

33 Y. Fazli, S. M. Pourmortazavi, I. Kohsari, M. S. Karimi and M. Tajdari, Synthesis, characterization and photocatalytic property of nickel sulfide nanoparticles, *J. Mater. Sci. Mater. Electron.*, 2016, **7**, 7192–7199, DOI: 10.1007/S10854-016-4683-2.

34 N. Jiang, Q. Tang, M. Sheng, B. You, D. E. Jiang and Y. Sun, Nickel sulfides for electrocatalytic hydrogen evolution under alkaline conditions: a case study of crystalline NiS, NiS_2, and Ni_3S_2 nanoparticles, *Catal. Sci. Technol.*, 2016, **6**, 1077–1084, DOI: 10.1039/C5CY01111F.

35 H. Li, L. Chai, X. Wang, X. Wu, G. Xi, Y. Liu and Y. Qian, Hydrothermal growth and morphology modification of β-NiS three-dimensional flowerlike architectures, *Cryst. Growth Des.*, 2007, **7**, 1918–1922, DOI: 10.1021/CG0703588/SUPPL_FILE/CG0703588.PDF.

36 A. Molla, M. Sahu and S. Hussain, Synthesis of tunable band gap semiconductor nickel sulphide nanoparticles: rapid and round the clock degradation of organic dyes, *Sci. Rep.*, 2016, **6**, 26034, DOI: 10.1038/SREP26034.

37 Q. Zhang, Y. Xiao, Y. Li, K. Zhao, H. Deng, Y. Lou, J. Chen and L. Cheng, NiS-decorated ZnO/ZnS nanorod heterostructures for enhanced photocatalytic hydrogen production: insight into the role of NiS, *Sol. RRL*, 2020, **4**, 1900568, DOI: 10.1002/SOLR.201900568.

38 A. Moulahi, Cu doped NiS/ZnS nanocomposites for photodegradation of methyl green, methylene blue and congo red pollutants, *J. Inorg. Organomet. Polym. Mater.*, 2023, 1–13, DOI: 10.1007/S10904-023-02702-Z/FIGURES/11.

39 M. Ramzan, M. Javed, S. Iqbal, A. Alhujaily, Q. Mahmood, K. Aroosh, A. Bahadur, M. A. Qayyum, N. S. Awwad, H. A. Ibrahium, M. M. Al-Anazy and E. B. Elkaeed, Designing highly active S-g-C_3N_4/Te@NiS ternary nanocomposites for antimicrobial performance, degradation of organic pollutants, and their kinetic study, *Inorganics*, 2023, **11**, 156, DOI: 10.3390/INORGANICS11040156/S1.

40 M. R. D. Khaki, M. S. Shafeeyan, A. A. A. Raman and W. M. A. W. Daud, Application of doped photocatalysts for organic pollutant degradation – a review, *J. Environ. Manage.*, 2017, **198**, 78–94, DOI: 10.1016/J.JENVMAN.2017.04.099.

41 X. Zheng, L. Wang, Y. Zhou, M. Luo, H. Li, Z. Bo, W. Zheng, C. Chang, J. Wen and J. Dong, *In situ* synthesis of NiS-modified MgO/S-doped biochar for boosting the adsorption-photocatalytic activity, *J. Ind. Eng. Chem.*, 2023, **126**, 492–500, DOI: 10.1016/J.JIEC.2023.06.037.

42 A. Manikandan, E. Hema, M. Durka, M. Amutha Selvi, T. Alagesan and S. Arul Antony, Mn^{2+} doped NiS ($Mn_xNi_{1-x}S$: $x = 0.0$, 0.3 and 0.5) nanocrystals: structural, morphological, opto-magnetic and photocatalytic properties, *J. Inorg. Organomet. Polym. Mater.*, 2015, **25**, 804–815, DOI: 10.1007/S10904-014-0163-4/TABLES/4.

43 Y. Yalçin, M. Kiliç and Z. Çinar, The role of non-metal doping in TiO_2 photocatalysis, *J. Adv. Oxid. Technol.*, 2010, **13**, 281–296, DOI: 10.1515/JAOTS-2010-0306/MACHINEREADABLECITATION/RIS.

44 C. Di Valentin and G. Pacchioni, Trends in non-metal doping of anatase TiO_2: B, C, N and F, *Catal. Today*, 2013, **206**, 12–18, DOI: 10.1016/J.CATTOD.2011.11.030.

45 M. Nasirian, Y. P. Lin, C. F. Bustillo-Lecompte and M. Mehrvar, Enhancement of photocatalytic activity of titanium dioxide using non-metal doping methods under visible light: a review, *Int. J. Environ. Sci. Technol.*, 2017, **159**(15), 2009–2032, DOI: 10.1007/S13762-017-1618-2.

46 F. Ling, W. Li and L. Ye, The synergistic effect of non-metal doping or defect engineering and interface coupling on the photocatalytic property of g-C_3N_4: first-principle investigations, *Appl. Surf. Sci.*, 2019, **473**, 386–392, DOI: 10.1016/J.APSUSC.2018.12.085.

47 W. Tang, X. Liu, Y. Li, Y. Pu, Y. Lu, Z. Song, Q. Wang, R. Yu and J. Shui, Boosting electrocatalytic water splitting *via* metal–metalloid combined modulation in quaternary Ni–Fe–P–B amorphous compound, *Nano Res.*, 2020, **13**, 447–454, DOI: 10.1007/S12274-020-2627-X/METRICS.

48 S. Gouse Peera, H. J. Kwon, T. G. Lee and A. M. Hussain, Heteroatom- and metalloid-doped carbon catalysts for oxygen reduction reaction: a mini-review, *Ionics*, 2020, **26**, 1563–1589, DOI: 10.1007/S11581-020-03473-0.

49 Q. U. Ain Asif, H. Asim, A. G. Nabi, M. Rehman, A. Shahzad, M. Kashif and A. Hussain, First-principles study of metals, metalloids and halogens doped monolayer $MoSe_2$ to tune its electronic properties, *Phys. Scr.*, 2023, **98**, 105917, DOI: 10.1088/1402-4896/ACF2CC.

50 K. Park, J. Kwon, S. Jo, S. Choi, E. Enkhtuvshin, C. Kim, D. Lee, J. Kim, S. Sun, H. S. Han and T. Song, Simultaneous electrical and defect engineering of nickel iron metal–organic-framework *via* co-doping of metalloid and non-metal elements for a highly efficient oxygen evolution reaction, *Chem. Eng. J.*, 2022, **439**, 135720, DOI: 10.1016/J.CEJ.2022.135720.

51 Z. Peng, S. Lou, Y. Gao, L. Kong, S. Yan, K. Wang and H. Song, Effect of co doping on electrocatalytic performance of co-nis2/cos2 heterostructures, *Nanomaterials*, 2021, **11**, 1245, DOI: 10.3390/NANO11051245/S1.

52 C. Wu, Y. Du, Y. Fu, D. Feng, H. Li, Z. Xiao, Y. Liu, Y. Yang and L. Wang, Mo, Co co-doped NiS bulks supported on Ni foam as an efficient electrocatalyst for overall water splitting in alkaline media, *Sustainable Energy Fuels*, 2020, **4**, 1654–1664, DOI: 10.1039/C9SE00822E.

53 L. L. Qian, Y. Li, J. feng Li and C. W. Wang, Enhanced photocatalytic performance from NiS/TiO_2 p–n heterojunction nanosheet arrays, *Superlattices Microstruct.*, 2018, **117**, 317–329, DOI: 10.1016/J.SPMI.2018.03.060.

54 V. Gadore, S. R. Mishra and M. Ahmaruzzaman, One-pot synthesis of CdS/CeO_2 heterojunction nanocomposite with tunable bandgap for the enhanced advanced oxidation process, *Sci. Rep.*, 2023, **13**, 7708, DOI: 10.1038/s41598-023-34742-3.

55 S. R. Mishra, V. Gadore and M. Ahmaruzzaman, Inorganic–organic hybrid quantum dots for AOP-mediated photodegradation of ofloxacin and para-nitrophenol in diverse water matrices, *NPJ Clean Water*, 2023, **61**(6), 1–24, DOI: 10.1038/s41545-023-00291-5.

56 D. Zhao and C. F. Yang, Recent advances in the TiO_2/CdS nanocomposite used for photocatalytic hydrogen production and quantum-dot-sensitized solar cells, *Renew. Sustainable Energy Rev.*, 2016, **54**, 1048–1059, DOI: 10.1016/J.RSER.2015.10.100.

57 Z. Zhang, Z. Fan, Q. Zhang and Y. Wang, Synthesis of flower-like 3NiS/$Zn_{0.5}Cd_{0.5}S$ high-efficiency composite catalysts, *Opt. Mater.*, 2021, **122**, 111681, DOI: 10.1016/J.OPTMAT.2021.111681.

58 Y. Yang, Q. Meng, X. Jiang, S. Meng, X. Zheng, S. Zhang, X. Fu and S. Chen, Photocatalytic performance of NiS/CdS composite with multistage structure, *ACS Appl. Energy Mater.*, 2020, **3**, 7736–7745, DOI: 10.1021/ACSAEM.0C01133/SUPPL_FILE/AE0C01133_SI_001.PDF.

59 R. Verma, S. R. Mishra, V. Gadore and M. Ahmaruzzaman, Hydroxyapatite-based composites: excellent materials for environmental remediation and biomedical applications, *Adv. Colloid Interface Sci.*, 2023, **315**, 102890, DOI: 10.1016/J.CIS.2023.102890.

60 S. R. Mishra, V. Gadore and M. Ahmaruzzaman, Influence of doped elements (O, K, and N) on melamine derived g-C_3N_4: insights into optical properties and photoactivity, *Int. J. Environ. Anal. Chem.*, 2023, DOI: 10.1080/03067319.2023.2260750.

61 S. Ranjan Mishra, V. Gadore and M. Ahmaruzzaman, Novel 3D sphere-like β-In2S3/Biochar nanoflowers for remediation of dyes in single and binary systems and interpretation using statistical physical modeling, *Environ. Nanotechnology, Monit. Manage.*, 2023, **20**, 100807, DOI: 10.1016/J.ENMM.2023.100807.

62 Z. Wang, H. Xia, P. Wang, X. Zhou, C. Liu, Q. Zhang, F. Wang, M. Huang, S. Chen, P. Wu, Y. Chen, J. Ye, S. Huang, H. Yan, L. Gu, J. Miao, T. Li, X. Chen, W. Lu, P. Zhou and W. Hu, Controllable doping in 2D layered materials, *Adv. Mater.*, 2021, **33**, 2104942, DOI: 10.1002/ADMA.202104942.

63 S. A. Abubshait, S. Iqbal, H. A. Abubshait, A. A. AlObaid, T. I. Al-Muhimeed, H. S. M. Abd-Rabboh, A. Bahadur and W. Z. Li, Effective heterointerface combination of 1D/2D Co-NiS/S-g-C_3N_4 heterojunction for boosting spatial charge separation with enhanced photocatalytic degradation of organic pollutants and disinfection of pathogens, *Colloids Surf., A*, 2021, **628**, 127390, DOI: 10.1016/J.COLSURFA.2021.127390.

64 G. Zhou, Z. Zhou, Y. Xia, W. Yin, J. Hou, X. Zhu, J. Yi, S. Wang, X. Ning and X. Wang, Synchronous synthesis of S-doped carbon nitride/nickel sulfide photocatalysts for efficient dye degradation and hydrogen evolution, *Appl. Surf. Sci.*, 2023, **608**, 154974, DOI: 10.1016/J.APSUSC.2022.154974.

65 M. Fiaz, M. Kashif, M. Fatima, S. R. Batool, M. A. Asghar, M. Shakeel and M. Athar, Synthesis of efficient TMS@MOF-5 catalysts for oxygen evolution reaction, *Catal. Lett.*, 2020, **150**, 2648–2659, DOI: 10.1007/S10562-020-03155-6/TABLES/2.

66 A. Nezamzadeh-Ejhieh and M. Khorsandi, Photodecolorization of eriochrome black T using NiS–P zeolite as a heterogeneous catalyst, *J. Hazard. Mater.*, 2010, **176**, 629–637, DOI: 10.1016/J.JHAZMAT.2009.11.077.

67 Z. xu Bi, R. tang Guo, X. yin Ji, X. Hu, J. Wang, X. Chen and W. guo Pan, Direct Z-scheme CoS/g-C_3N_4 heterojunction with NiS co-catalyst for efficient photocatalytic hydrogen generation, *Int. J. Hydrogen Energy*, 2022, **47**, 34430–34443, DOI: 10.1016/J.IJHYDENE.2022.08.028.

68 F. Soofivand, E. Esmaeili, M. Sabet and M. Salavati-Niasari, Simple synthesis, characterization and investigation of photocatalytic activity of NiS_2 nanoparticles using new precursors by hydrothermal method, *J. Mater. Sci. Mater. Electron.*, 2018, **29**, 858–865, DOI: 10.1007/S10854-017-7981-4/FIGURES/8.

69 P. Mohammadyari and A. Nezamzadeh-Ejhieh, Supporting of mixed ZnS–NiS semiconductors onto clinoptilolite nanoparticles to improve its activity in photodegradation of 2-nitrotoluene, *RSC Adv.*, 2015, **5**, 75300–75310, DOI: 10.1039/C5RA12608H.

70 S. Kokilavani, A. A. Al-Kheraif, A. M. Thomas, A. Syed, A. M. Elgorban, L. L. Raju, A. Das and S. S. Khan, Novel NiS/Ag_2MoO_4 heterostructure nanocomposite: synthesis, characterization and superior antibacterial and enhanced photocatalytic activity, *Phys. E*, 2021, **133**, 114767, DOI: 10.1016/J.PHYSE.2021.114767.

71 H. J. Khadim, A. Al-Farraji and S. H. Ammar, Boosted visible-light-driven photocatalytic degradation of lomefloxacin over α-Ag_2WO_4/NiS_x nanocomposites, *Environ. Nanotechnol. Monit. Manage.*, 2022, **18**, 100722, DOI: 10.1016/J.ENMM.2022.100722.

72 G. C. Zhang, J. Zhong, M. Xu, Y. Yang, Y. Li, Z. Fang, S. Tang, D. Yuan, B. Wen and J. Gu, Ternary $BiVO_4$/NiS/Au nanocomposites with efficient charge separations for enhanced visible light photocatalytic performance, *Chem. Eng. J.*, 2019, **375**, 122093, DOI: 10.1016/J.CEJ.2019.122093.

73 H. Derikvandi and A. Nezamzadeh-Ejhieh, Comprehensive study on enhanced photocatalytic activity of heterojunction ZnS-NiS/zeolite nanoparticles: experimental design based on response surface methodology (RSM), impedance

spectroscopy and GC-MASS studies, *J. Colloid Interface Sci.*, 2017, **490**, 652–664, DOI: **10.1016/J.JCIS.2016.11.105**.

74 Y. N. Luo, J. L. Dong, Z. J. Jiang, X. Q. Zhang, Y. Li and C. W. Wang, β-$Ni(OH)_2$/NiS/TiO_2 3D flower-like p–n–p heterostructural photocatalysts for high-efficiency removal of soluble anionic dyes and hydrogen releasing, *Opt. Mater.*, 2021, **114**, 110951, DOI: **10.1016/J.OPTMAT.2021.110951**.

75 N. Kandhasamy, G. Murugadoss, T. Kannappan, K. Kirubaharan, R. K. Manavalan and R. Gopal, Cerium-based metal sulfide derived nanocomposite-embedded rGO as an efficient catalyst for photocatalytic application, *Environ. Sci. Pollut. Res.*, 2023, **30**, 29711–29726.

76 P. H. Mahmood, O. Amiri, S. S. Ahmed and J. R. Hama, Simple microwave synthesis of TiO_2/NiS_2 nanocomposite and TiO_2/NiS_2/Cu nanocomposite as an efficient visible driven photocatalyst, *Ceram. Int.*, 2019, **45**, 14167–14172, DOI: **10.1016/J.CERAMINT.2019.04.118**.

77 T. Mohlala, T. L. Yusuf and N. Mabuba, Photoelectrocatalytic degradation of emerging organic pollutants in water on an FTO/$BiVO_4$/NiS photoanode, *J. Electroanal. Chem.*, 2023, **947**, 117806, DOI: **10.1016/J.JELECHEM.2023.117806**.

78 B. Harikumar, M. K. Okla, I. A. Alaraidh, A. Mohebaldin, W. Soufan, M. A. Abdel-Maksoud, M. Aufy, A. M. Thomas, L. L. Raju and S. S. Khan, Robust visible light active $CoNiO_2$–$BiFeO_3$–NiS ternary nanocomposite for photo-fenton degradation of rhodamine B and methyl orange: kinetics, degradation pathway and toxicity assessment, *J. Environ. Manage.*, 2022, **317**, 115321, DOI: **10.1016/J.JENVMAN.2022.115321**.

79 E. M. Khudhair, S. H. Ammar, S. Z. Al-Najjar, S. M. Al-Jubouri, A. S. Mahdi and Z. H. Jabbar, Facile construction of g-C_3N_4/$MnWO_4$/NiS heterostructures for photocatalytic degradation of organic contaminates under visible light irradiation, *Mater. Lett.*, 2023, **347**, 134599, DOI: **10.1016/J.MATLET.2023.134599**.

80 F. Jamal, A. Rafique, S. Moeen, J. Haider, W. Nabgan, A. Haider, M. Imran, G. Nazir, M. Alhassan, M. Ikram, Q. Khan, G. Ali, M. Khan, W. Ahmad and M. Maqbool, Review of metal sulfide nanostructures and their applications, *ACS Appl. Nano Mater.*, 2023, **6**, 7077–7106, DOI: **10.1021/ACSANM.3C00417/ASSET/IMAGES/MEDIUM/AN3C00417_0026.GIF**.

81 V. Gadore and M. M. Ahmaruzzaman, Fly ash-based nanocomposites: a potential material for effective photocatalytic degradation/elimination of emerging organic pollutants from aqueous stream, *Environ. Sci. Pollut. Res.*, 2021, **28**, 46910–46933, DOI: **10.1007/s11356-021-15251-0**.

82 S. R. Mishra, V. Gadore and M. Ahmaruzzaman, Insights into persulfate-activated photodegradation of tinidazole and photoreduction of hexavalent chromium through β-In2S3 anchored on Ag-doped fish scale-derived HAp composite quantum dots, *J. Clean. Prod.*, 2023, **427**, 139221, DOI: **10.1016/J.JCLEPRO.2023.139221**.